On the Discretization of Linear Fractional Representations of LPV Systems

R. Tóth, *Member, IEEE*, M. Lovera, *Member, IEEE*, P. S. C. Heuberger, M. Corno and P. M. J. Van den Hof, *Fellow, IEEE*

Abstract

Commonly, controllers for Linear Parameter-Varying (LPV) systems are designed in continuous time using a Linear Fractional Representation (LFR) of the plant. However, the resulting controllers are implemented on digital hardware. Furthermore, discrete-time LPV synthesis approaches require a discrete-time model of the plant which is often derived from a continuous-time first-principle model. Existing discretization approaches for LFRs describing LPV systems suffer from disadvantages like the possibility of serious approximation errors, issues of complexity, etc. To explore the disadvantages, existing discretization methods are reviewed and novel approaches are derived to overcome them. The proposed and existing methods are compared and analyzed in terms of approximation error, considering ideal zero-order hold actuation and sampling. Criteria to choose appropriate sampling times with respect to the investigated methods are also presented. The proposed discretization methods are tested and compared both on a simulation example and on the electronic throttle control problem of a race motorcycle.

Index Terms

Linear fractional representation; discretization; linear parameter-varying systems.

I. Introduction

Control synthesis approaches for *linear parameter-varying* (LPV) systems (e.g., [1]–[3]), often require LPV models in a *linear fractional representation* (LFR), as depicted in Fig. 1. In the LPV interpretation of LFRs, the feedback gain Δ is assumed to vary in time as Δ is a function

R. Tóth, P. S. C. Heuberger, M. Corno and P. M. J. Van den Hof are with the Delft Center for Systems and Control, Delft University of Technology, Mekelweg 2, 2628 CD, Delft, The Netherlands, email: {r.toth, p.s.c.heuberger, m.corno, p.m.j.vandenhof}@tudelft.nl.

M. Lovera is with the Dipartimento di Elettronica e Informazione, Politecnico di Milano, Piazza Leonardo da Vinci 20133, Milano, Italy, email: lovera@elet.polimi.it.

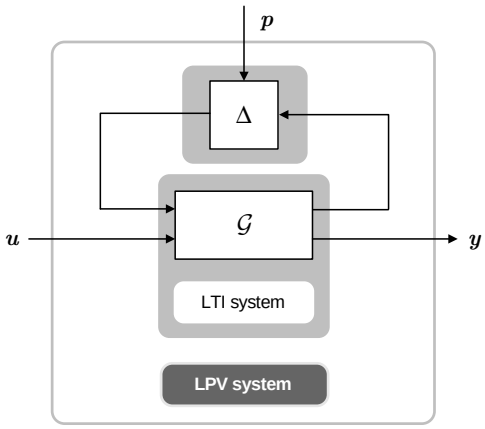

Fig. 1. Linear fractional representation of LPV systems.

of a time-dependent measurable signal, the so-called *scheduling variable* $p : \mathbb{R} \to \mathbb{P}$. The compact set (or polytope) $\mathbb{P} \subset \mathbb{R}^{n_\mathbb{P}}$ denotes the so called *scheduling 'space'*. Using scheduling variables to represent changing operating conditions or endogenous/free signals of the plant, LPV representations can describe both nonlinear and time-varying phenomena. Note that LFRs of LPV systems can be seen as a generalization of LFRs of uncertain LTI systems where Δ is assumed to be a constant or a time-varying uncertainty. By treating these uncertainties as scheduling variables, such descriptions blend into the framework considered in this paper.

In practice, implementation of LPV controllers in physical hardware generally meets significant difficulties, as often *continuous-time* (CT) LPV control synthesis approaches [2] are preferred in the literature over *discrete-time* (DT) methods [1]. The main reason is that stability and performance requirements can be more conveniently expressed in CT, like in a mixed sensitivity setting [3]. Therefore, the current design tools focus on CT-LPV controller synthesis in an LFR form, requiring efficient discretization of such system representations for implementation purposes. Next to that, DT approaches require a DT model of the plant which is often available only through the use of CT first-principle models. It follows that discretization of LFR representations of LPV systems is a crucial issue for both control design and implementation.

In the existing literature, some approaches to LFR discretization are available. However, the validity of the used discretization settings or the introduced approximation error has not been analyzed so far. Moreover, only the isolated, i.e. stand alone discretization of the LFR's is treated. Note that similar to the LTI case, the plant and its controller needs to be discretized

together (non-isolated setting) if the objective is to preserve the performance of the control loop [4]. Basically the available methods use *zero-order hold* (ZOH) and *first-order hold* (1OH) approaches to restrict the variations of the signals of the LFR in the sampling interval which results in a DT description of the dynamics [5]–[12]. Almost all of these methods suffer from various disadvantages like the possibility of significant approximation error, loss of stability, high complexity etc., see Sec. III. Furthermore there are also important questions that need to be thoroughly investigated, for example the choice of the *sampling period*, such that a specified discretization error and/or preservation of the stability characteristics can be guaranteed.

For the sake of completeness it is important to note, that LFR's are in fact special *differential algebraic equations* (DAE's) and hence existing DAE discretization (solution) methods (see e.g. [13]–[15]) can be applied on them. However, using these general approaches it is either not possible to reconstruct a DT LFR or they are too general (concentrating on high index DAE's) to provide transparent results where the above stated questions can be investigated.

In this paper we aim to analyze discretization settings for LPV models in the LFR case and to derive exact extensions of the approaches of the LTI framework. We compare the properties of the resulting approaches in terms of preservation of stability and discretization errors. By taking the first step towards a systematic discretization theory, we restrict the focus in this paper to the isolated setting. We will return to this issue at the end of the paper, showing that preservation of closed-loop performance in the LPV case also requires a non-isolated approach and in this respect the current results of the paper offer a well-founded starting point towards such solutions.

The current paper extends the results reported in [16] and is organized as follows: first, in Sec. II, LFRs of LPV systems are defined. Existing approaches to LFR discretization are investigated in Sec. III, pointing out the need for improvement. Using an exact discretization setting in Sec. IV, traditional discretization methods of the LTI framework are extended to LFRs. In Sec. V, properties of the introduced methods are presented in terms of discretization error and preservation of stability. In Sec. VI, both a simulation example and a real life LPV throttle control problem of a race motorcycle are investigated to demonstrate the performance and properties of the proposed approaches. Finally the conclusions of the paper are presented in Sec. VII.

II. Linear Fractional Representations

The LFR of a given continuous-time LPV system $\mathcal{S}$ is denoted by $\mathfrak{R}_{\mathrm{LFR}}(\mathcal{S})$ and defined as

$$\begin{bmatrix} \dot{x}(t) \\ z(t) \\ y(t) \end{bmatrix} = \begin{bmatrix} A & B_1 & B_2 \\ C_1 & D_{11} & D_{12} \\ C_2 & D_{21} & D_{22} \end{bmatrix} \begin{bmatrix} x(t) \\ w(t) \\ u(t) \end{bmatrix} \tag{1a}$$

where $u : \mathbb{R} \to \mathbb{U} = \mathbb{R}^{n_{\mathrm{u}}}$ and $y : \mathbb{R} \to \mathbb{Y} = \mathbb{R}^{n_{\mathrm{y}}}$ are the input and output signals of the system $\mathcal{S}$, containing disturbance/actuated input and measurable/unmeasurable output channels alike. $x : \mathbb{R} \to \mathbb{X} = \mathbb{R}^{n_{\mathrm{x}}}$ is the state variable of the representation. $\{A, \ldots, D_{22}\}$ are constant matrices with appropriate dimensions and

$$w(t) = \Delta(p)(t)\, z(t), \tag{1b}$$

where Δ is an operator working on the scheduling signal p of $\mathcal{S}$ and resulting in a matrix valued signal, i.e. $\Delta(p)(t) \in \mathbb{R}^{n_{\mathrm{w}} \times n_{\mathrm{z}}}$. Commonly, Δ has a block diagonal structure containing the elements of $p(t)$ and Δ is assumed to vary in a convex polytope. Note that (1a-b) is a DAE, instead of an *ordinary differential equation* (ODE) encountered in state-space representations. Additionally, x, w, z are latent (auxiliary) variables of $\mathfrak{R}_{\mathrm{LFR}}(\mathcal{S})$.

By defining y_{d}, u_{d}, p_{d} as the sampled signals of y, u, p with *sampling period* $\mathtt{T}_{\mathrm{d}} > 0$, e.g., $u_{\mathrm{d}}(k) := u(k\mathtt{T}_{\mathrm{d}})$, the definition of a LFR can be established in DT as the representation of an underlying sampled continuous-time LPV system $\mathcal{S}$:

$$\begin{bmatrix} x_{\mathrm{d}}(k+1) \\ z_{\mathrm{d}}(k) \\ y_{\mathrm{d}}(k) \end{bmatrix} = \begin{bmatrix} \Phi & \Gamma_1 & \Gamma_2 \\ \Upsilon_1 & \Omega_{11} & \Omega_{12} \\ \Upsilon_2 & \Omega_{21} & \Omega_{22} \end{bmatrix} \begin{bmatrix} x_{\mathrm{d}}(k) \\ w_{\mathrm{d}}(k) \\ u_{\mathrm{d}}(k) \end{bmatrix} \tag{2}$$

where $\{\Phi, \ldots, \Omega_{22}\}$ are constant matrices with appropriate dimensions and

$$w_{\mathrm{d}}(k) = \Delta_{\mathrm{d}}(p_{\mathrm{d}})(k)\, z_{\mathrm{d}}(k), \tag{3}$$

with $\Delta_{\mathrm{d}}(p_{\mathrm{d}})(k) \in \mathbb{R}^{n_{\mathrm{w_d}} \times n_{\mathrm{z_d}}}$. Note that it is not necessary that z_{d}, w_{d}, or x_{d} are also sampled signals of their CT counterparts (they are just latent variables). In the sequel, this representation is denoted as $\mathfrak{R}_{\mathrm{LFR}}(\mathcal{S}, \mathtt{T}_{\mathrm{d}})$. It is important to note that depending on $\mathtt{T}_{\mathrm{d}}$, the existence of $\mathfrak{R}_{\mathrm{LFR}}(\mathcal{S}, \mathtt{T}_{\mathrm{d}})$ is not guaranteed. On the other hand, not every DT-LFR corresponds to a sampled CT-LFR as discrete-time systems and representations are self-standing mathematical concepts. However, here we are interested in the relations between DT and CT descriptions and the possibility of preserving the dynamical behavior through a DT projection.

Now we can define the problem we intend to focus on in the rest of the paper:

Problem 1 (Discretization problem): For a sampling period $\mathtt{T}_\mathrm{d} > 0$ and for a given LFR of a CT-LPV system $\mathcal{S}$, find a DT-LFR that describes or approximates the sampled behavior of the output signal y of $\mathcal{S}$ in terms of a given error measure and a threshold for all possible trajectories of the input u and the scheduling variable p. □

III. Existing discretization approaches

Before deriving a solution to Problem 1, the existing LFR discretization approaches are investigated by evaluating their performance in terms of the proposed problem setting and also pointing out the need for improvements.

A. Basic concepts of the discretization settings

In the available literature, only the isolated setting (stand alone discretization of the system) is treated. Similar to the LTI case, in this setting it is necessary to restrict the free variables of the system, i.e., u and p, to vary in a predefined manner during fixed time intervals, called the *sampling intervals*. This is required in order to describe the continuous-time evolution of all non-free variables inside these time intervals. Having an exact characterization of these trajectories makes it possible to derive a DT description of the system where signals are only observed at the end of the sampling interval, i.e., with the sampling period $\mathtt{T}_\mathrm{d}$. The simplest case is when a *zero-order-hold* (ZOH) device is applied on u and p, restricting their variation to be piecewise-constant. However, this restriction can be relaxed to include a larger set of possible signal trajectories like piece-wise linear (called *first-order-hold*), or 2^{nd}-order polynomial (called *second-order-hold*), etc. In order to simplify the discretization problem we face in this setting, the following assumption is commonly used (see [17]):

Assumption 1 (Discretization setting): The hold and the sampling devices are perfectly synchronized with $\mathtt{T}_\mathrm{d} > 0$ as the *sampling period* or *discretization time step*. Furthermore, these devices have infinite resolution (no quantization error) and their processing time is zero. □

Note that due to the assumed ideal hold devices, at the beginning of each sampling interval a switching effect occurs. Contrary to the LTI case, the switching effect on p introduces additional dynamics into the system which are not present in the original CT behavior. To avoid the overcomplicated analysis of such effects, the following assumption is made:

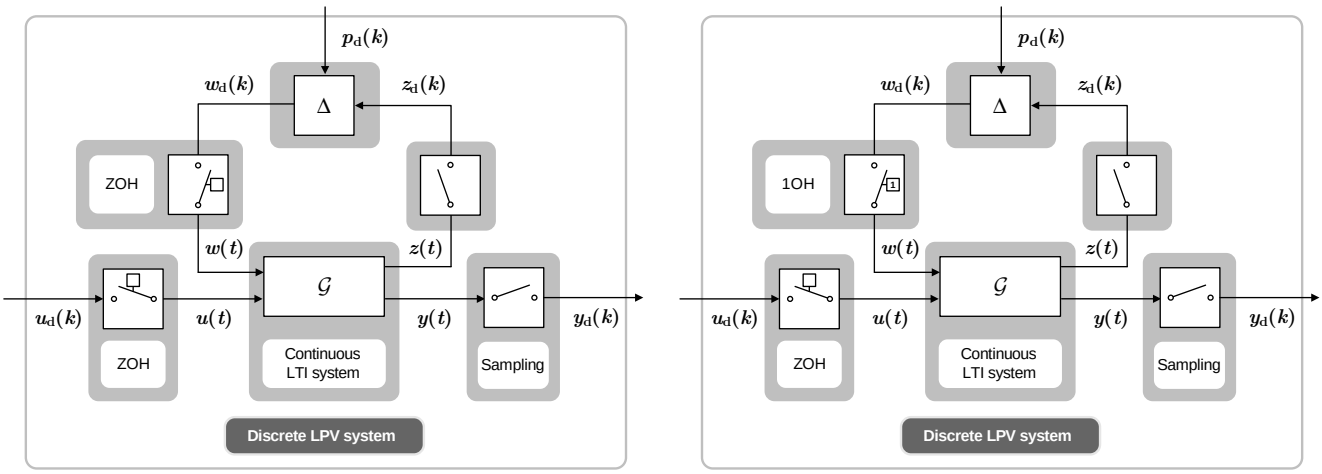

Fig. 2. (a) Full ZOH discretization of LFRs. (b) First/Zero-order hold discretization of LFRs.

Assumption 2 (Switching effects): The switching behavior of the hold devices has no effect on the CT plant, i.e., the switching of the signals is assumed to take place smoothly.

B. Full zero-order hold approaches

A commonly used approach, like in [5], [6], is to apply ZOHs and sampling on all signals of (1a-b) (see Fig. 2a). This setting implies that (1a) is discretized as a stand-alone (open-loop) LTI system disregarding (1b). The advantage of this method lays in its simplicity, however it can seriously alter the dynamics, i.e., stability, of the DT approximation as it assumes that all terms in the state equation that are coupled with Δ are constant inside the sampling interval. To demonstrate the latter property consider the following example:

Example 1: Suppose that a CT-LFR is given as

$$\begin{bmatrix} \dot{x}(t) \\ z(t) \\ y(t) \end{bmatrix} = \begin{bmatrix} 0 & -1 & 1 \\ 1 & 0 & 0 \\ 1 & 0 & 0 \end{bmatrix} \begin{bmatrix} x(t) \\ w(t) \\ u(t) \end{bmatrix} \tag{4}$$

with $w(t) = \Delta(p)(t)z(t)$, $\Delta(p)(t) = p(t)$ and $0 < \mathtt{p}_{\min} \leq p(t) \leq \mathtt{p}_{\max}$. Then

$$\dot{x}(t) = -\overbrace{p(t)x(t)}^{w(t)} + u(t), \tag{5a}$$

$$y(t) = x(t), \tag{5b}$$

and $z(t) = x(t)$. Based on a Lyapunov argument, it follows that (5a) is asymptotically stable (see [18]). Now by applying the ZOH in terms of Fig. 2a we have:

$$u(t) = u(k\mathtt{T}_\mathrm{d}) \quad \text{and} \quad w(t) = p(k\mathtt{T}_\mathrm{d})x(k\mathtt{T}_\mathrm{d}), \tag{6}$$

for $t \in [k\mathtt{T}_\mathrm{d}, (k+1)\mathtt{T}_\mathrm{d})$. From (5a) it follows that

$$x(t) = x(k\mathtt{T}_\mathrm{d}) + \int_{k\mathtt{T}_\mathrm{d}}^{t} \big(-w(\tau) + u(\tau)\big)\, \mathrm{d}\tau = x(k\mathtt{T}_\mathrm{d}) + \int_{k\mathtt{T}_\mathrm{d}}^{t} \big(-p(k\mathtt{T}_\mathrm{d})x(k\mathtt{T}_\mathrm{d}) + u(k\mathtt{T}_\mathrm{d})\big)\, \mathrm{d}\tau, \tag{7}$$

for $t \in [k\mathtt{T}_\mathrm{d}, (k+1)\mathtt{T}_\mathrm{d})$. It is obvious that the integral is over a constant function (no state variation), thus

$$x((k+1)\mathtt{T}_\mathrm{d}) = (1 - \mathtt{T}_\mathrm{d} p(k\mathtt{T}_\mathrm{d}))x(k\mathtt{T}_\mathrm{d}) + \mathtt{T}_\mathrm{d} u(k\mathtt{T}_\mathrm{d}), \tag{8}$$

implying the DT-LFR:

$$\begin{bmatrix} x_\mathrm{d}(k+1) \\ z_\mathrm{d}(k) \\ y_\mathrm{d}(k) \end{bmatrix} = \begin{bmatrix} 1 & -\mathtt{T}_\mathrm{d} & \mathtt{T}_\mathrm{d} \\ 1 & 0 & 0 \\ 1 & 0 & 0 \end{bmatrix} \begin{bmatrix} x_\mathrm{d}(k) \\ w_\mathrm{d}(k) \\ u_\mathrm{d}(k) \end{bmatrix} \tag{9}$$

with $\Delta_\mathrm{d}(p_\mathrm{d})(k) = p(k\mathtt{T}_\mathrm{d})$. The corresponding DT system is asymptotically stable if $\mathtt{T}_\mathrm{d} < \frac{2}{\mathtt{p}_{\max}}$ (see [18]). This illustrates that the original dynamics of the plant are substituted by a piecewise linear evolution of the state in this discretization setting hence the stability characteristics are altered.

C. First/Zero-order hold approaches

Other methods, like [7], [8], use a mixed discretization setting of first and zero-order holds, depicted in Fig. 2b. By considering future samples of p and z in terms of the 1OH, the approximation of the variations of x that are coupled with Δ improves. However, this also often turns out to be a disadvantage, as the resulting DT-LFR depends on future samples of p and w, which results in a non-causal representation. In case the ultimate goal of the discretization is analysis or simulation, this causality problem might not be disadvantageous (see [7]). For demonstration, consider the CT-LFR given in Example 1.

Example 2: In the setting of Fig. 2b, (4) implies that

$$w(t) = p(k\mathtt{T}_\mathrm{d})x(k\mathtt{T}_\mathrm{d}) + \frac{t - k\mathtt{T}_\mathrm{d}}{\mathtt{T}_\mathrm{d}} \Big(p((k+1)\mathtt{T}_\mathrm{d})x((k+1)\mathtt{T}_\mathrm{d}) - p(k\mathtt{T}_\mathrm{d})x(k\mathtt{T}_\mathrm{d})\Big), \tag{10}$$

and $u(t) = u(k\mathtt{T}_\mathrm{d})$ for $t \in [k\mathtt{T}_\mathrm{d}, (k+1)\mathtt{T}_\mathrm{d})$. By computing the state evolution (7) inside the sampling interval one obtains (see [18] for the detailed derivation)

$$\left(1 + \frac{\mathtt{T}_\mathrm{d}}{2} p((k+1)\mathtt{T}_\mathrm{d})\right) x((k+1)\mathtt{T}_\mathrm{d}) = \left(1 - \frac{\mathtt{T}_\mathrm{d}}{2} p(k\mathtt{T}_\mathrm{d})\right) x(k\mathtt{T}_\mathrm{d}) + \mathtt{T}_\mathrm{d} u(k\mathtt{T}_\mathrm{d}), \tag{11}$$

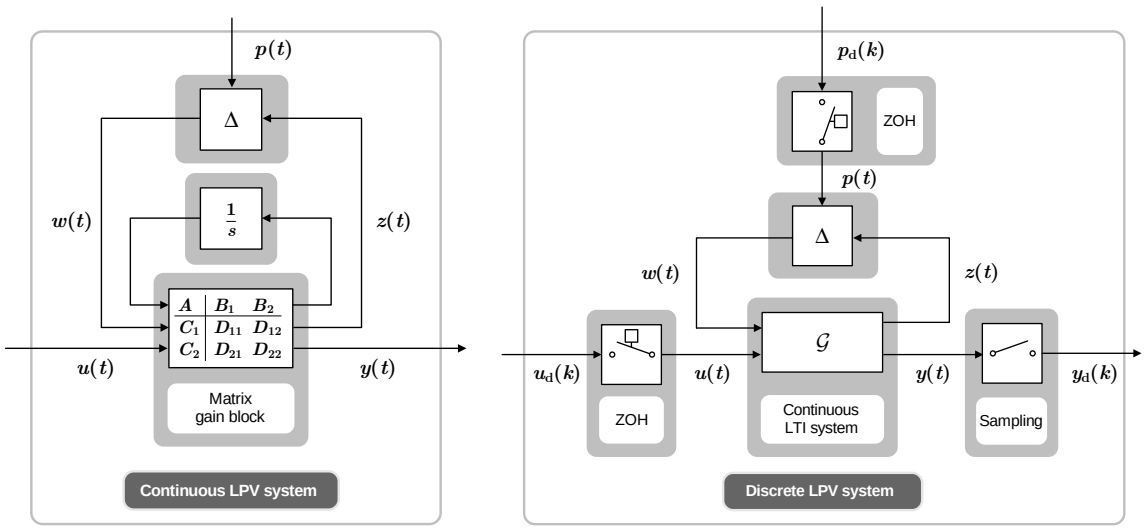

(a) (b)

Fig. 3. (a) Extraction of the integrator for bilinear discretization. (b) Exact ZOH discretization of LFRs.

which implies the DT-LFR:

$$\begin{bmatrix} x_{\mathrm{d}}(k+1) \\ z_{\mathrm{d}}(k) \\ y_{\mathrm{d}}(k) \end{bmatrix} = \left[\begin{array}{c:cc:c} 1 & -\frac{\mathtt{T}_{\mathrm{d}}}{2} & -\frac{\mathtt{T}_{\mathrm{d}}}{2} & \mathtt{T}_{\mathrm{d}} \\ \hdashline 1 & -\frac{\mathtt{T}_{\mathrm{d}}}{2} & -\frac{\mathtt{T}_{\mathrm{d}}}{2} & \mathtt{T}_{\mathrm{d}} \\ \hdashline 1 & 0 & 0 & 0 \\ \hdashline 1 & 0 & 0 & 0 \end{array}\right] \begin{bmatrix} x_{\mathrm{d}}(k) \\ w_{\mathrm{d}}(k) \\ u_{\mathrm{d}}(k) \end{bmatrix} \tag{12}$$

with $\Delta_{\mathrm{d}}(p_{\mathrm{d}})(k) = \left[\begin{smallmatrix} p((k+1)\mathtt{T}_{\mathrm{d}}) & 0 \\ 0 & p(k\mathtt{T}_{\mathrm{d}}) \end{smallmatrix}\right]$. It can be proven that even if arbitrarily fast variation of p_{d} is allowed, i.e., $p \in \mathbb{P}^{\mathbb{Z}}$, (11) is asymptotically stable for any $\mathtt{T}_{\mathrm{d}} > 0$ (see [18]). (11) gives a rational approximation of the original state evolution, better than (8), but with a price of non-causality[1] in the p-dependence and an increase in the dimensions of Δ_{d}.

D. Bilinear transformation technique

As an alternative, the time operator in the state-equation can be extracted as an integrator (see Fig. 3a) which is discretized via the z-substitution of its Laplace transform $1/s$ (see [9], [10]). For the substitution, the bilinear transformation

$$\frac{1}{s} \approx \frac{\mathtt{T}_{\mathrm{d}}}{2}\frac{z+1}{z-1}, \tag{13}$$

is used, resulting in a Tustin type of discretization approach. It can be shown that this intuitive

[1]Note that in this simple example it is possible to introduce a p-dependent state transformation to eliminate the non-causal dependence. However, such an elimination is not possible in general [7], [8].

method introduces ZOH only on u and p, depicted in Fig. 3b, and it does not restrict variations of the state. Furthermore, this concept preserves stability of the original representation. On the other hand, the formulation of the approach is only based on the analogy with the LTI case and it does not give an understanding of the introduced approximations. To demonstrate this method, again consider the previously investigated example.

Example 3: The bilinear transformation (13) corresponds to the evaluation of the integral (7) by the trapezoidal formula. Using the nonlinear state transformation

$$\breve{x}_{\mathrm{d}}(k) = \frac{1}{\sqrt{\mathtt{T}_{\mathrm{d}}}} x(k\mathtt{T}_{\mathrm{d}}) + \frac{\sqrt{\mathtt{T}_{\mathrm{d}}}}{2} w(k\mathtt{T}_{\mathrm{d}}) - \frac{\sqrt{\mathtt{T}_{\mathrm{d}}}}{2} u(k\mathtt{T}_{\mathrm{d}}), \tag{14}$$

the resulting DT-LFR is

$$\begin{bmatrix} \breve{x}_{\mathrm{d}}(k+1) \\ z_{\mathrm{d}}(k) \\ y_{\mathrm{d}}(k) \end{bmatrix} = \begin{bmatrix} 1 & -\sqrt{\mathtt{T}_{\mathrm{d}}} & \sqrt{\mathtt{T}_{\mathrm{d}}} \\ \sqrt{\mathtt{T}_{\mathrm{d}}} & -\frac{1}{2}\mathtt{T}_{\mathrm{d}} & \frac{1}{2}\mathtt{T}_{\mathrm{d}} \\ \sqrt{\mathtt{T}_{\mathrm{d}}} & -\frac{1}{2}\mathtt{T}_{\mathrm{d}} & \frac{1}{2}\mathtt{T}_{\mathrm{d}} \end{bmatrix} \begin{bmatrix} \breve{x}_{\mathrm{d}}(k) \\ w_{\mathrm{d}}(k) \\ u_{\mathrm{d}}(k) \end{bmatrix} \tag{15}$$

with $\Delta_{\mathrm{d}}(p_{\mathrm{d}})(k) = p_{\mathrm{d}}(k)$ (see [9]). Using a Lyapunov argument, it can be shown that this DT-LFR is asymptotically stable for any $\mathtt{T}_{\mathrm{d}} > 0$ and trajectories of $p_{\mathrm{d}} : \mathbb{Z} \to [\mathtt{p}_{\min}, \mathtt{p}_{\max}]$ (see [18]).

E. Discretization in state-space form

Another discretization approach is to rewrite (1a-b) as an LPV *state-space* (SS) representation:

$$\dot{x} = \mathcal{A}(p)x + \mathcal{B}(p)u, \tag{16a}$$

$$y = \mathcal{C}(p)x + \mathcal{D}(p)u. \tag{16b}$$

This reformulation is possible if the following (well-posedness) condition holds:

Assumption 3: $I - D_{11}\Delta(p)$ is invertible for all $p \in \mathbb{P}^{\mathbb{R}}$ and $t \in \mathbb{R}$. □

In (16a-b) the matrices are given as (see e.g. [3])

$$\mathcal{A}(p) = A + B_1\Delta(p)(I - D_{11}\Delta(p))^{-1}C_1, \tag{17a}$$

$$\mathcal{B}(p) = B_2 + B_1\Delta(p)(I - D_{11}\Delta(p))^{-1}D_{12}, \tag{17b}$$

$$\mathcal{C}(p) = C_2 + D_{21}\Delta(p)(I - D_{11}\Delta(p))^{-1}C_1, \tag{17c}$$

$$\mathcal{D}(p) = D_{22} + D_{21}\Delta(p)(I - D_{11}\Delta(p))^{-1}D_{12}. \tag{17d}$$

As a next step, the discretization formulas of LPV-SS representations derived in [11], [12] are applied on (16a-b). Then, the resulting discrete-time LPV-SS representation is transformed to a discrete-time LFR. This approach provides a wide range of fully analyzed methods with criteria

for the choice of the sampling period. However, conversion between LFR and SS representations is complicated and the resulting DT-SS representations might not be realizable by an LFR without introducing conservatism (see Sec. IV-A).

F. Concluding remarks

The above given overview of the available approaches suggests that the applied discretization setting in itself determines the quality of the achievable DT approximation. We have seen that some approaches suffer from serious approximation errors and alteration of the stability characteristics of the original system. The best properties follow from the setting of Fig. 3 as the state variation in the sampling interval is not restricted. However, the applied Tustin method only provides an approximation, raising the question: can we do more in the setting of Fig. 3? In the sequel we intend to focus on this question and extend other successful discretization approaches for LFR representations similar to the case of LPV-SS representations (see [11]). We analyze when it is possible to give an errorless DT projection and how the error introduced by approximative methods can be determined. As we will see, this yields criteria for the choice of $\mathtt{T}_\mathrm{d}$ to preserve stability and to achieve a desired performance with the introduced approaches.

IV. Exact ZOH discretization of LFRs

Based on the previous conclusions, we will investigate whether an approximation-free solution to Problem 1 exists in the ZOH setting presented in Fig. 3b and if such a method can provide a practically useful DT projection of CT-LFRs of LPV systems. The following assumption is introduced:

Assumption 4 (exact ZOH setting): We are given a CT-LPV system $\mathcal{S}$, with CT input signal u, scheduling signal p, and output signal y, where u and p are generated by an ideal ZOH device and y is sampled. Additionally, the ZOHs and the sampling satisfy Assumptions 1-2 with $\mathtt{T}_\mathrm{d} > 0$. □

These assumptions imply that for $k \in \mathbb{Z}$

$$u(t) := u_\mathrm{d}(k), \quad \forall t \in [k\mathtt{T}_\mathrm{d}, (k+1)\mathtt{T}_\mathrm{d}), \tag{18a}$$

$$p(t) := p_\mathrm{d}(k), \quad \forall t \in [k\mathtt{T}_\mathrm{d}, (k+1)\mathtt{T}_\mathrm{d}), \tag{18b}$$

$$y_\mathrm{d}(k) := y(k\mathtt{T}_\mathrm{d}). \tag{18c}$$

A. Complete approach

First the complete signal evolution approach [17] of the LTI framework is extended to the LFR case. Let a CT-LFR be given in the ZOH setting of Fig. 3b. Based on Assumption 4, (1a) can be written as

$$\begin{bmatrix} \dot{x}(t) \\ z(t) \\ y(t) \end{bmatrix} = \begin{bmatrix} A & B_1\Delta(p)(k\mathtt{T_d}) & B_2 \\ C_1 & D_{11}\Delta(p)(k\mathtt{T_d}) & D_{12} \\ C_2 & D_{21}\Delta(p)(k\mathtt{T_d}) & D_{22} \end{bmatrix} \begin{bmatrix} x(t) \\ z(t) \\ u(k\mathtt{T_d}) \end{bmatrix} \tag{19}$$

which corresponds to a DAE. Now in the k^{th} sampling interval, $x(t)$ reads as

$$x(t) = x(k\mathtt{T_d}) + \int_{k\mathtt{T_d}}^{t} Ax(\tau) + B_1\Delta(p)(k\mathtt{T_d})z(\tau) + B_2u(k\mathtt{T_d})\ \mathrm{d}\tau, \quad \forall t \in [k\mathtt{T_d}, (k+1)\mathtt{T_d}). \tag{20}$$

If Assumption 3 holds, then (19) is an index-0 DAE, meaning that its solution can be obtained by algebraically eliminating the latent variable z to obtain an ODE form. Then, for $t = (k+1)\mathtt{T_d}$, (20) yields

$$x((k+1)\mathtt{T_d}) = e^{\mathtt{T_d}\mathcal{A}(p)(k\mathtt{T_d})}x(k\mathtt{T_d}) + \mathcal{A}^{-1}(p)(k\mathtt{T_d})\left(e^{\mathtt{T_d}\mathcal{A}(p)(k\mathtt{T_d})} - I\right)\mathcal{B}(p)(k\mathtt{T_d})u(k\mathtt{T_d}). \tag{21}$$

Note that invertibility of $\mathcal{A}(p)$ is not required for obtaining the solution (nor for the calculation of the resulting matrix functions), but if it is invertible, we can write the resulting DT description of the sate-evolution conveniently as (21). This solution implies a DT realization of the original system, however as $e^{\mathtt{T_d}\mathcal{A}(p)}$ is not a rational function of $\Delta(p)$, it is not possible to find an exact DT-LFR which describes the state transition from $(x(k\mathtt{T_d}), u(k\mathtt{T_d}))$ to $x((k+1)\mathtt{T_d})$ defined by (21). One option is to introduce

$$\Delta_{\mathrm{d}}(p_{\mathrm{d}})(k) = \begin{bmatrix} \Delta(p)(k\mathtt{T_d}) & 0 \\ 0 & e^{\mathtt{T_d}\mathcal{A}(p)(k\mathtt{T_d})} \end{bmatrix}, \tag{22}$$

and provide a DT-LFR realization of (21), which however might be rather unattractive for controller synthesis due to issues of conservatism.

Now consider the case when Assumption 3 is not satisfied[2]. Then, (19) is an index-1 DAE, meaning that its solution (if it exists) can only be obtained by differentiating (19) once. In general, such solution also has no exact DT-LFR realization.

These conclusions underline that unlike the LTI and the LPV-SS cases, no exact DT projection of the dynamics is available in the LFR case under Assumption 4.

[2]Note that invertibility of $I - D_{11}\Delta(p)$ is only a sufficient but not a necessary condition for the well-posedness of LFRs (see [19]).

B. Approximative approaches

As we have seen, complete discretization of LFRs is rather difficult, thus it is important to develop approximative methods. By looking at the state-equation of (1a) as a pure ODE, numerical approximations of the resulting CT solution can be applied. Then, by using the algebraic constraints in (1a-b), a DT-LFR can be obtained that approximates the original behavior under Assumption 4. In the literature on numerical methods, such an approach is reported to work well for DAE's with index 0 and 1. Using this methodology, the following approximative methods can be derived:

1) Rectangular (Euler's forward) method: Denote the righthand-side of the state equation in (1a) by $f(x,w,u)$, so

$$f(x,w,u)(t) = Ax(t) + B_1 w(t) + B_2 u(t). \tag{23}$$

Then,

$$x(t) = x(k\mathtt{T}_\mathrm{d}) + \int_{k\mathtt{T}_\mathrm{d}}^{t} f(x,w,u)(\tau)\ \mathrm{d}\tau \tag{24}$$

defines the state evolution of (1a) in $[k\mathtt{T}_\mathrm{d}, (k+1)\mathtt{T}_\mathrm{d})$. Left-hand rectangular evaluation of (24) gives that

$$x((k+1)\mathtt{T}_\mathrm{d}) \approx x(k\mathtt{T}_\mathrm{d}) + \mathtt{T}_\mathrm{d} f(x,w,u)(k\mathtt{T}_\mathrm{d}). \tag{25}$$

Based on this rectangular approach, the DT approximation of $\mathfrak{R}_{\mathrm{LFR}}(\mathcal{S})$ reads as

$$\mathfrak{R}_{\mathrm{LFR}}(\mathcal{S}, \mathtt{T}_\mathrm{d}) \approx \begin{bmatrix} I + \mathtt{T}_\mathrm{d} A & \mathtt{T}_\mathrm{d} B_1 & \mathtt{T}_\mathrm{d} B_2 \\ C_1 & D_{11} & D_{12} \\ C_2 & D_{21} & D_{22} \end{bmatrix}, \tag{26}$$

with $\Delta_\mathrm{d}(p_\mathrm{d})(k) = \Delta(p)(k\mathtt{T}_\mathrm{d})$ (see [18]). Note that using a first-order Taylor approximation of $e^{\mathtt{T}_\mathrm{d}\mathcal{A}(p(k\mathtt{T}_\mathrm{d}))}$ in (21) (which is called the Euler method) results in the same DT-LFR realization as (26). It is also important to highlight that the rectangular approach gives the same solution as the full ZOH setting of Fig. 2a with Euler discretization of the LTI part, suggesting very poor performance for this method. Therefore, by applying the rectangular method on the previously considered example, the resulting DT description reads as (9).

2) Polynomial (Hanselmann) method: It is possible to develop other methods that achieve a better approximation of the complete solution (21) but with increasing complexity. One way leads through the use of higher-order Taylor expansions of the matrix exponential:

$$e^{\mathtt{T}_\mathrm{d}\mathcal{A}(p)(k\mathtt{T}_\mathrm{d})} \approx I + \textstyle\sum_{l=1}^{n} \frac{\mathtt{T}_\mathrm{d}^l}{l!} \mathcal{A}^l(p)(k\mathtt{T}_\mathrm{d}). \tag{27}$$

This gives the following DT-LFR (see [18]):

$$\mathfrak{R}_{\mathrm{LFR}}(\mathcal{S},\mathtt{T_d}) \approx \left[\begin{array}{c|c|c|c|c|c} \sum_{l=0}^{n} \frac{\mathtt{T_d}^l}{l!}A^l & \sum_{l=1}^{n} \frac{\mathtt{T_d}^l}{l!}A^{l-1}B_1 & \sum_{l=2}^{n} \frac{\mathtt{T_d}^l}{l!}A^{l-2}B_1 & \dots & \frac{\mathtt{T_d}^n}{n!}B_1 & \sum_{l=1}^{n} \frac{\mathtt{T_d}^l}{l!}A^{l-1}B_2 \\ \hline C_1 & D_{11} & 0 & \dots & 0 & D_{12} \\ C_1A & C_1B_1 & D_{11} & \dots & 0 & C_1B_2 \\ \vdots & \vdots & \ddots & \ddots & \vdots & \vdots \\ C_1A^{n-1} & C_1A^{n-2}B_1 & C_1A^{n-3}B_1 & \dots & D_{11} & C_1A^{n-1}B_2 \\ \hline C_2 & D_{21} & 0 & \dots & 0 & D_{22} \end{array}\right] \tag{28}$$

with $\Delta_{\mathrm{d}}(p_{\mathrm{d}})(k) = I_{n\times n} \otimes \Delta(p)(k\mathtt{T_d})$ where $\otimes$ is the Kronecker product. Additionally, the above defined method is not equivalent to applying polynomial discretization of the LTI part in the spirit of Fig. 2a. Considering the previously given example, the polynomial method with $n = 2$ results in the following DT approximation of (4):

$$\left[\begin{array}{c} x_{\mathrm{d}}(k+1) \\ z_{\mathrm{d}}(k) \\ y_{\mathrm{d}}(k) \end{array}\right] = \left[\begin{array}{c|ccc} 1 & -\mathtt{T_d} & -\frac{\mathtt{T_d}^2}{2} & \mathtt{T_d} \\ \hline 1 & 0 & 0 & 0 \\ 0 & -1 & 0 & 1 \\ \hline 1 & 0 & 0 & 0 \end{array}\right] \left[\begin{array}{c} x_{\mathrm{d}}(k) \\ w_{\mathrm{d}}(k) \\ u_{\mathrm{d}}(k) \end{array}\right] \tag{29}$$

which is asymptotically stable if $\mathtt{T_d} < \frac{2}{\mathtt{p}_{\max}}$ (see [18]).

3) Padé's expansion method: A different way of approximating the exponential term in (21), is to use a rational approximation in the form of a Padé (i, j) expansion:

$$e^{\mathtt{T_d}\mathcal{A}(p)} \approx [T_{ij}(\mathtt{T_d}\mathcal{A}(p))]^{-1}\, N_{ij}(\mathtt{T_d}\mathcal{A}(p)), \tag{30}$$

where

$$T_{ij}(\mathtt{T_d}\mathcal{A}(p)) = \textstyle\sum_{l=0}^{j} \frac{(i+j-l)!j!}{(i+j)!l!(j-l)!} \left(-\mathtt{T_d}\mathcal{A}(p)\right)^l, \tag{31a}$$

$$N_{ij}(\mathtt{T_d}\mathcal{A}(p)) = \textstyle\sum_{l=0}^{i} \frac{(i+j-l)!i!}{(i+j)!l!(i-l)!} \left(\mathtt{T_d}\mathcal{A}(p)\right)^l. \tag{31b}$$

In general, (30) has a much faster convergence rate than (27). Approximation of matrix exponentials by Padé expansions is also viewed as an attractive approach in the numerical literature [20], [21]. Substituting (30) into (21) gives

$$T_{ij}(\mathtt{T_d}\mathcal{A}(p)(k\mathtt{T_d}))x((k+1)\mathtt{T_d}) \approx N_{ij}(\mathtt{T_d}\mathcal{A}(p)(k\mathtt{T_d}))x(k\mathtt{T_d}) + \hat{N}_{ij}(\mathtt{T_d}\mathcal{A}(p)(k\mathtt{T_d}))\mathcal{B}(p)(k\mathtt{T_d})u(k\mathtt{T_d}), \tag{32}$$

where, for $i = j$,

$$\hat{N}_{ii}(\mathtt{T_d}\mathcal{A}(p)) = \mathcal{A}(p)^{-1}\big(N_{ii}(\mathtt{T_d}\mathcal{A}(p)) - T_{ii}(\mathtt{T_d}\mathcal{A}(p))\big). \tag{33}$$

As T_{ij}, N_{ij} and $\hat{N}_{ij}$ are rational functions of $\Delta(p)$, there exists a DT-LFR realization of (32). In the case $i = j = 1$, $T_{11}(\mathtt{T}_\mathrm{d}\mathcal{A}(p)(k\mathtt{T}_\mathrm{d})) = I - \frac{\mathtt{T}_\mathrm{d}}{2}\mathcal{A}(p)(k\mathtt{T}_\mathrm{d})$ and $N_{11}(\mathtt{T}_\mathrm{d}\mathcal{A}(p)(k\mathtt{T}_\mathrm{d})) = I + \frac{\mathtt{T}_\mathrm{d}}{2}\mathcal{A}(p)(k\mathtt{T}_\mathrm{d})$, giving that a minimal DT-LFR realization of (32) reads as (see [18])

$$\mathfrak{R}_{\mathrm{LFR}}(\mathcal{S}, \mathtt{T}_\mathrm{d}) \approx \left[\begin{array}{c:cc:c} (I + \frac{\mathtt{T}_\mathrm{d}}{2}A)\Psi & \frac{\mathtt{T}_\mathrm{d}}{2}\Psi B_1 & \frac{\mathtt{T}_\mathrm{d}}{2}\Psi B_1 & \mathtt{T}_\mathrm{d}\Psi B_2 \\ \hdashline C_1(I + \frac{\mathtt{T}_\mathrm{d}}{2}A)\Psi & \frac{\mathtt{T}_\mathrm{d}}{2}C_1\Psi B_1 + D_{11} & \frac{\mathtt{T}_\mathrm{d}}{2}C_1\Psi B_1 & \mathtt{T}_\mathrm{d}C_1\Psi B_2 + D_{12} \\ C_1 & 0 & D_{11} & D_{12} \\ \hdashline C_2 & 0 & D_{21} & D_{22} \end{array}\right] \tag{34}$$

with $\Psi = (I - \frac{\mathtt{T}_\mathrm{d}}{2}A)^{-1}$ and $\Delta_\mathrm{d}(p_\mathrm{d})(k) = I_{2\times 2} \otimes \Delta(p)(k\mathtt{T}_\mathrm{d})$. Again, it is important to note that the above defined method is not equivalent to the Padé discretization of the LTI part in the spirit of Fig. 2a. Considering the previously given example, the Padé's expansion method with $(i, j) = (1, 1)$ results in the following DT approximation of (4):

$$\left[\begin{array}{c} x_\mathrm{d}(k+1) \\ z_\mathrm{d}(k) \\ y_\mathrm{d}(k) \end{array}\right] = \left[\begin{array}{c:cc:c} 1 & -\frac{\mathtt{T}_\mathrm{d}}{2} & -\frac{\mathtt{T}_\mathrm{d}}{2} & \mathtt{T}_\mathrm{d} \\ \hdashline 1 & -\frac{\mathtt{T}_\mathrm{d}}{2} & -\frac{\mathtt{T}_\mathrm{d}}{2} & \mathtt{T}_\mathrm{d} \\ 1 & 0 & 0 & 0 \\ \hdashline 1 & 0 & 0 & 0 \end{array}\right] \left[\begin{array}{c} x_\mathrm{d}(k) \\ w_\mathrm{d}(k) \\ u_\mathrm{d}(k) \end{array}\right]. \tag{35}$$

It can be easily proven that the above given LFR is asymptotically stable for any $\mathtt{T}_\mathrm{d} > 0$ and any trajectory of $p_\mathrm{d} : \mathbb{Z} \to [\mathtt{p}_{\min}, \mathtt{p}_{\max}]$ (see [18]).

4) Trapezoidal (Tustin) method: Another approach is to use different numerical formulas to approximate (24). By using a trapezoidal evaluation, we obtain:

$$x((k+1)\mathtt{T}_\mathrm{d}) \approx x(k\mathtt{T}_\mathrm{d}) + \tfrac{\mathtt{T}_\mathrm{d}}{2} f|_{k\mathtt{T}_\mathrm{d}} + \tfrac{\mathtt{T}_\mathrm{d}}{2} f|_{(k+1)\mathtt{T}_\mathrm{d}}, \tag{36}$$

where $f|_t = f(x, w, u)(t)$. Now by applying a change of variables:

$$\breve{x}_\mathrm{d}(k) = \tfrac{1}{\sqrt{\mathtt{T}_\mathrm{d}}}\left(I - \tfrac{\mathtt{T}_\mathrm{d}}{2}A\right) x(k\mathtt{T}_\mathrm{d}) - \tfrac{\sqrt{\mathtt{T}_\mathrm{d}}}{2} B_1 w(k\mathtt{T}_\mathrm{d}) - \tfrac{\sqrt{\mathtt{T}_\mathrm{d}}}{2} B_2 u(k\mathtt{T}_\mathrm{d}), \tag{37}$$

and assuming that $I - \frac{\mathtt{T}_\mathrm{d}}{2}A$ is invertible, substitution of (37) into (36) gives the DT-LFR:

$$\mathfrak{R}_{\mathrm{LFR}}(\mathcal{S}, \mathtt{T}_\mathrm{d}) \approx \left[\begin{array}{ccc} \left(I + \frac{\mathtt{T}_\mathrm{d}}{2}A\right)\Psi & \sqrt{\mathtt{T}_\mathrm{d}}\Psi B_1 & \sqrt{\mathtt{T}_\mathrm{d}}\Psi B_2 \\ \sqrt{\mathtt{T}_\mathrm{d}}C_1\Psi & \frac{\mathtt{T}_\mathrm{d}}{2}C_1\Psi B_1 + D_{11} & \frac{\mathtt{T}_\mathrm{d}}{2}C_1\Psi B_2 + D_{12} \\ \sqrt{\mathtt{T}_\mathrm{d}}C_2\Psi & \frac{\mathtt{T}_\mathrm{d}}{2}C_2\Psi B_1 + D_{21} & \frac{\mathtt{T}_\mathrm{d}}{2}C_2\Psi B_2 + D_{22} \end{array}\right] \tag{38}$$

with $\Delta_\mathrm{d}(p_\mathrm{d})(k) = \Delta(p)(k\mathtt{T}_\mathrm{d})$ and $\Psi = (I - \frac{\mathtt{T}_\mathrm{d}}{2}A)^{-1}$. The trapezoidal approach exactly gives the same solution as the bilinear method introduced in Sec. III-D. Therefore, by applying this method to the previously considered example, the resulting DT description reads as in Sec. III-D.

5) Multi-step methods: (24) can also be approximated via multi-step formulas like the Runge-Kutta, Adams-Moulton, or the Adams-Bashforth approaches [13]. However, in the considered ZOH discretization setting, the sampling period is fixed and sampled data is only available at past and present sampling instants. Therefore it is complicated to apply the Runge-Kutta or the Adams-Moulton approaches. The family of Adams-Bashforth methods, on the other hand, does fulfill these requirements (see [13]). The 3-step version of this numerical approach uses the following approximation of $x((k+1)\mathtt{T}_\mathrm{d})$:

$$x(k\mathtt{T}_\mathrm{d}) + \frac{\mathtt{T}_\mathrm{d}}{12}\left(5f|_{(k-2)\mathtt{T}_\mathrm{d}} - 16f|_{(k-1)\mathtt{T}_\mathrm{d}} + 23f|_{k\mathtt{T}_\mathrm{d}}\right). \tag{39}$$

Then introducing a new state variable

$$\breve{x}_\mathrm{d}(k) = \begin{bmatrix} x^\top(k\mathtt{T}_\mathrm{d}) & f|_{(k-1)\mathtt{T}_\mathrm{d}}^\top & f|_{(k-2)\mathtt{T}_\mathrm{d}}^\top \end{bmatrix}^\top \tag{40}$$

leads to the DT-LFR (see [18]):

$$\mathfrak{R}_{\mathrm{LFR}}(\mathcal{S}, \mathtt{T}_\mathrm{d}) \approx \left[\begin{array}{ccc:c:c} I + \frac{23\mathtt{T}_\mathrm{d}}{12}A & -\frac{16\mathtt{T}_\mathrm{d}}{12}I & \frac{5\mathtt{T}_\mathrm{d}}{12}I & \frac{23\mathtt{T}_\mathrm{d}}{12}B_1 & \frac{23\mathtt{T}_\mathrm{d}}{12}B_2 \\ A & 0 & 0 & B_1 & B_2 \\ 0 & I & 0 & 0 & 0 \\ \hdashline C_1 & 0 & 0 & D_{11} & D_{12} \\ \hdashline C_2 & 0 & 0 & D_{21} & D_{22} \end{array}\right] \tag{41}$$

with $\Delta_\mathrm{d}(p_\mathrm{d})(k) = \Delta(p)(k\mathtt{T}_\mathrm{d})$. Note that multi-step discretization results in simple formulas but the state dimension is increased. Applying this method for the previous example results in

$$\begin{bmatrix} \breve{x}_\mathrm{d}(k+1) \\ z_\mathrm{d}(k) \\ y_\mathrm{d}(k) \end{bmatrix} = \left[\begin{array}{ccc:c:c} 1 & -\frac{16\mathtt{T}_\mathrm{d}}{12} & \frac{5\mathtt{T}_\mathrm{d}}{12} & -\frac{23\mathtt{T}_\mathrm{d}}{12} & \frac{23\mathtt{T}_\mathrm{d}}{12} \\ 0 & 0 & 0 & -1 & 1 \\ 0 & 1 & 0 & 0 & 0 \\ \hdashline 1 & 0 & 0 & 0 & 0 \\ \hdashline 1 & 0 & 0 & 0 & 0 \end{array}\right] \begin{bmatrix} \breve{x}_\mathrm{d}(k) \\ w_\mathrm{d}(k) \\ u_\mathrm{d}(k) \end{bmatrix} \tag{42}$$

for which asymptotic stability can only be analyzed numerically for a specific $\mathbb{P}$.

V. Properties of the approaches

A. Numerical properties and discretization error

Using a similar line of reasoning as in [11], [12], the discretization error of the introduced approaches can be investigated through their numerical properties. In this section we will briefly cover how these properties and error bounds apply for the discretization methods of Sec. IV.

1) Local discretization error: Due to the approximative nature of the discretization methods developed in Section IV-B it is important to characterize the quality of approximation for example in terms of the approximation error of the state evolution. For this purpose the concept of *Local Unit Truncation* (LUT) error, denoted by $\varepsilon_k \in \mathbb{R}^{n_\mathrm{x}}$, is introduced. Let $R_\mathrm{x}(q,p_\mathrm{d})$ and $R_\mathrm{u}(q,p_\mathrm{d})$ be polynomials in q with p_d-dependent coefficient matrices. Choose these polynomials such that they formulate the state update of the DT approximations on the same state basis as in the original CT-LFR: $\mathfrak{R}_\mathrm{LFR}(\mathcal{S})$. In the rectangular, polynomial and the Padé cases, $R_\mathrm{x}(q,p_\mathrm{d}) = \mathcal{A}_\mathrm{d}(p_\mathrm{d})$ and $R_\mathrm{u}(q,p_\mathrm{d}) = \mathcal{B}_\mathrm{d}(p_\mathrm{d})$, where $\mathcal{A}_\mathrm{d}$ and $\mathcal{B}_\mathrm{d}$ are computed according to (17a-d) for the DT-LFR form, but in the other cases, they also include the appropriate state transformation. For example, in the trapezoidal case, (36) describes the DT state update w.r.t. the original state basis of $\mathfrak{R}_\mathrm{LFR}(\mathcal{S})$. By using the change of variables (37), we transformed (36) to correspond to an LFR state equation. However in terms of analysis we need (36) to characterize the LUT error w.r.t. x_d. This gives rise to polynomials

$$R_\mathrm{x}(q,p_\mathrm{d})(k) = I + \tfrac{\mathtt{T}_\mathrm{d}}{2}\mathcal{A}(p_\mathrm{d})(k) + \tfrac{\mathtt{T}_\mathrm{d}}{2}\mathcal{A}(qp_\mathrm{d})(k)q,$$
$$R_\mathrm{u}(q,p_\mathrm{d})(k) = \tfrac{\mathtt{T}_\mathrm{d}}{2}\mathcal{B}(p_\mathrm{d})(k) + \tfrac{\mathtt{T}_\mathrm{d}}{2}\mathcal{B}(qp_\mathrm{d})(k)q,$$

in the Trapezoidal case and

$$R_\mathrm{x}(q,p_\mathrm{d})(k) = \left(I + \tfrac{23}{12}\mathtt{T}_\mathrm{d}\mathcal{A}(q^2p_\mathrm{d})(k)\right)q^2 - \tfrac{16}{23}\mathtt{T}_\mathrm{d}\mathcal{A}(qp_\mathrm{d})(k)q + \tfrac{5}{23}\mathtt{T}_\mathrm{d}\mathcal{A}(p_\mathrm{d})(k),$$
$$R_\mathrm{u}(q,p_\mathrm{d})(k) = \tfrac{23}{12}\mathtt{T}_\mathrm{d}\mathcal{B}(q^2p_\mathrm{d})(k)q^2 - \tfrac{16}{23}\mathtt{T}_\mathrm{d}\mathcal{B}(qp_\mathrm{d})(k)q + \tfrac{5}{23}\mathtt{T}_\mathrm{d}\mathcal{B}(p_\mathrm{d})(k),$$

in the Adams-Bashforth case.

By using the introduced polynomials, ε_k is defined by

$$T_\mathrm{d}\varepsilon_{k+n} := \left(q^n x_\mathrm{d} - R_\mathrm{x}(q,p_\mathrm{d})x_\mathrm{d} - R_\mathrm{u}(q,p_\mathrm{d})u_\mathrm{d}\right)(k), \tag{43}$$

for each sampling interval. In (43), $n = 1$ for all single step methods (all considered approaches except the Adams-Bashforth case) while n equals to the number of steps in case of a multi-step method (like $n = 3$ for the 3-step Adams-Bashforth method). Note that LUT represents the relative (scaled by $\mathtt{T}_\mathrm{d}$) approximation error of the system dynamics at each sampling period, when the correct sampled continuous states x and inputs u are used for the state update of the DT approximation. Hence the name ”local”. In the theory of numerical approximation of differential equations, ε_k is considered as the measure of accuracy [13]. Based on simple calculations, the LUT error of each method can be characterized and formulas can be given to calculate an

upper bound of its norm (see [11] for the details). Based on these expressions of the LUT error, it follows that the derived methods are numerically consistent and convergent, which means that by decreasing $\mathtt{T}_\mathrm{d}$ the approximation error of the sampled CT behavior also converges to zero. Furthermore, the order of numerical convergence (the lowest order of derivative of x being necessary to bound the LUT error) indicates the convergence rate of this error (see [13]). The rate of convergence is given in the first row of Table I for each method. Methods with high convergence rate, like the polynomial and Padé approaches, provide more accurate approximations (with decreasing $\mathtt{T}_\mathrm{d}$) than the other methods. However convergence in terms of the LUT error does not imply that the *global approximation error*

$$\eta_{k+n} := \big(q^n x_\mathrm{d} - R_\mathrm{x}(q, p_\mathrm{d})\hat{x}_\mathrm{d} - R_\mathrm{u}(q, p_\mathrm{d})u_\mathrm{d}\big)(k), \tag{44}$$

where n is the number of steps in the approximation method and $\hat{x}_\mathrm{d}$ is the DT approximation of the state, decreases/converges to zero too. In terms of practical applications, bounds on η_k have paramount importance.

2) Stability preservation: Preservation of stability through the discrete time projection can also be analyzed. Consider the CT-LFR (1a-b). For a constant trajectory of p, i.e., $p(t) \equiv \mathtt{p}$ for all $t \in \mathbb{R}$, $\mathcal{A}(p)$ is a constant matrix ((1a-b) reduces to a LTI system). We call (1a-b) uniformly frozen stable if (1a-b) is asymptotically stable for all constant trajectories of p. In terms of Assumption 2, this means that $\mathcal{A}(\mathtt{p})$ is Hurwitz for all $\mathtt{p} \in \mathbb{P}$. An analogous definition of frozen stability can be given for DT-LFRs. By analyzing the numerical stability of the DT projection (see [11]), it can be concluded that the preservation of uniform frozen stability of the CT-LFR is always guaranteed with the trapezoidal and the Padé approaches. With respect to other methods, analytic bounds $\breve{\mathtt{T}}_\mathrm{d}$ on the sampling period can be given for which preservation of frozen stability is guaranteed.

3) Adequate discretization step size: In practical situations, the appropriate choice of $\mathtt{T}_\mathrm{d}$ to arrive at a specific performance in terms of discretization error is important. By using the characterization of the LUT error, upper bounds of $\mathtt{T}_\mathrm{d}$ can be derived that guarantee a certain bound on the approximation error in terms of a chosen measure $\|\centerdot\|$. Define ε_* as the supremum of $\|\varepsilon_k\|$ over all possible state trajectories of $\mathfrak{R}_\mathrm{LFR}(\mathcal{S})$ and $k \in \mathbb{Z}$. Also introduce

$$M_\mathtt{x}^\mathrm{max} = \sup_x \max_{t\in\mathbb{R}} \|x\,(t)\| = \max_{\mathtt{x}\in\mathbb{X}} \|\mathtt{x}\|\,, \tag{45}$$

Property	Complete	Rectangular	n^{th}-polynomial	Trapezoidal	Padé (n,n)	Adams-Bashforth
consistency / convergence	always	1^{st}-order	n^{th}-order	2^{nd}-order	n^{th}-order	3^{rd}-order
preservation of stability / N-stab.	always	frozen with $\breve{\mathtt{T}}_{\mathrm{d}}$	frozen with $\breve{\mathtt{T}}_{\mathrm{d}}$	always frozen	always frozen	frozen with $\breve{\mathtt{T}}_{\mathrm{d}}$
preservation of instability	+	-	-	+	+	-
Δ_{d}-block complexity	not realizable	$1 \times \Delta$	$n \times \Delta$	$1 \times \Delta$	$2n \times \Delta$	$1 \times \Delta$
system order	preserved	preserved	preserved	preserved	preserved	increased

TABLE I

PROPERTIES OF THE DERIVED DISCRETIZATION METHODS

as the maximum "amplitude" of the state signal for any u and p. Also define $\varepsilon_{\max}$ as the required maximum relative local error of the discretization in terms of percentage. Then a $\mathtt{T}_{\mathrm{d}} > 0$ is searched for that satisfies

$$\varepsilon_* \leq \frac{\varepsilon_{\max} M_{\mathtt{x}}^{\max}}{100 \cdot \mathtt{T}_{\mathrm{d}}}. \tag{46}$$

By using the bounds on the LUT error derived in [11], we can formulate an upper bound of $\mathtt{T}_{\mathrm{d}}$ denoted as $\hat{\mathtt{T}}_{\mathrm{d}}$ w.r.t. each method, such that (46) is satisfied for the desired $\varepsilon_{\max}$ percentage. Note that, to derive these criteria, (45) must be bounded, i.e., $\mathbb{X}$ must be confined in a ball (bounded region) of $\mathbb{R}^{n_{\mathtt{x}}}$, which is not an unrealistic assumption in case of asymptotic stability of (1a-b) for all $p \in \mathbb{P}^{\mathbb{Z}}$) and bounded $\mathbb{P}$ and $\mathbb{U}$. In case of the Padé (i,j) approach, exact computation of $\hat{\mathtt{T}}_{\mathrm{d}}$ corresponds to a heavy nonlinear optimization problem, however the result can be approximated in a lower bound sense by the performance bound of the $(i+j)$-order polynomial method.

In practical situations one may be concerned about the maximum of the global error η_k (44) as a performance measure. Define η_* as the supremum of $\|\eta_k\|$ over all possible state trajectories of $\mathfrak{R}_{\mathrm{LFR}}(\mathcal{S})$ and $k \in \mathbb{Z}$. Also define $\eta_{\max}$ as the maximal acceptable relative global error of the discretization in terms of percentage. Then one would like to choose $\mathtt{T}_{\mathrm{d}}$ such that

$$\eta_* \leq \frac{\eta_{\max} M_{\mathtt{x}}^{\max}}{100}. \tag{47}$$

Unfortunately, characterization of η_* for the introduced discretization methods requires serious restrictions on the considered CT behaviors. However, in case of $\mathtt{T}_{\mathrm{d}} \leq \breve{\mathtt{T}}_{\mathrm{d}}$, $\varepsilon_{\max}$ can be used as a good approximation of $\eta_{\max}$, and therefore the performance bound $\hat{\mathtt{T}}_{\mathrm{d}}$ can be used to bound the global error as well.

B. Complexity of Δ_{d}

As in LPV control synthesis mostly low complexity (dimension, type of dependence, structure, etc.) of Δ is preferred (see [2]), therefore both for modeling and controller discretization purposes - beside the preservation of stability - the preservation of the original Δ without repetition is highly valued. This favors approximative methods that give acceptable performance, but with less repetition of Δ in the new Δ_{d} block. For the rectangular, trapezoidal and the Adams-Bashforth methods $\Delta_{\mathrm{d}} = \Delta$, making these approaches attractive from this point of view. However, in the Adams-Bashforth case, discretization also results in the order increase of the DT system which yields extra computational load or requires more complicated controller design depending on the intended use.

C. Overall assessment

If the quality of the DT model has priority, then the trapezoidal, polynomial, and the Padé methods are suggested due to their fast convergence and large stability radius. The Padé (n, n)-method is especially attractive as it merges the good properties of the trapezoidal and polynomial approaches like preservation of stability and fast convergence rate for high n. However the price to be paid is an increased number of repetitions of the Δ block. The above stated properties also clearly point out that there exists no 'best' discretization method as in specific scenarios one approach can be more attractive than the others. The choice of the method that is the most attractive w.r.t. the problem at hand will always be up to the user and may for instance be based on Table I.

VI. Examples

In the following a simple example is presented to visualize/compare the properties of the analyzed discretization methods. This will be followed by a more involved example of discretization of a LPV controller designed on the throttle body model of a race motorcycle and assessing the achieved closed loop performance of the resulting DT controller.

A. Simulation study of a simple LPV model

Consider the following LFR of a continuous-time SISO LPV system $\mathcal{S}$:

$$\mathfrak{R}_{\mathrm{LFR}}(\mathcal{S}) = \left[\begin{array}{cc:cc:c} 66 & -136 & 1 & 0 & 1 \\ 116 & -86 & 0 & 1 & 1 \\ \hdashline -58 & 123 & 0 & 0 & 1 \\ -10 & 75 & 0 & 0 & 1 \\ \hdashline 1 & 1 & -0.1 & -0.1 & 0.1 \end{array}\right]$$

with $\Delta(p) = \left[\begin{smallmatrix} p & 0 \\ 0 & p \end{smallmatrix}\right]$ and $\mathbb{P} = [-1, 1]$. For each constant scheduling trajectory, $\mathfrak{R}_{\mathrm{LFR}}(\mathcal{S})$ is equivalent to a stable LTI system, so $\mathcal{S}$ is uniformly frozen stable on $\mathbb{P}$.

Consider $\mathfrak{R}_{\mathrm{LFR}}(\mathcal{S})$ in the exact ZOH setting of Fig. 3b with sampling period $\mathtt{T}_{\mathrm{d}} = 0.02$ s. By applying the discretization methods of Sec. IV, approximative DT-LFRs of $\mathcal{S}$ have been calculated. For comparison, the full ZOH approach has also been applied on $\mathfrak{R}_{\mathrm{LFR}}(\mathcal{S})$. To demonstrate the performance of the resulting DT descriptions, the output of the original system and its DT approximations have been simulated on the time interval $[0, 1]$ with zero initial conditions and for 100 different realizations of white u_{d} and p_{d} with uniform distribution $\mathcal{U}(-1, 1)$. For fair comparison, the achieved (average) MSE[3] of the resulting output signals $\hat{y}_{\mathrm{d}}$ has been calculated w.r.t. the output y of $\mathfrak{R}_{\mathrm{LFR}}(\mathcal{S})$ and is presented in Table II. The relative worst-case maximum local error $\hat{\varepsilon}_{\max} = 100 \cdot \mathtt{T}_{\mathrm{d}} \varepsilon_* / M_{\mathtt{x}}^{\max}$ and global error $\hat{\eta}_{\max} = 100 \cdot \eta_* / M_{\mathtt{x}}^{\max}$ of the DT state-signals $\hat{x}_{\mathrm{d}}$ associated with the DT representations have also been computed w.r.t. x of $\mathfrak{R}_{\mathrm{LFR}}(\mathcal{S})$ and presented in Table II. For the calculation of $M_{\mathtt{x}}^{\max}$ it has been assumed that $\mathbb{X} = [-0.4, 0.4]^2$, which has been verified by simulations of $\mathfrak{R}_{\mathrm{LFR}}(\mathcal{S})$ based on $u_{\mathrm{d}}, p_{\mathrm{d}} \in \mathcal{U}(-1, 1)$ and $x(0) = [\ 0 \quad 0\ ]^\top$.

Table II shows that - except for the rectangular, polynomial and the Adams-Bashforth methods - all approximations converge. As expected, the error of the complete method is extremely small while the trapezoidal and the Padé $(1, 1)$ methods give a moderate, but acceptable performance. Surprisingly, the full ZOH approach also gives a stable projection with an acceptable error. This underlines that the full ZOH approach can provide effective discretization of LFRs in some cases. However, its weakness is its unpredictable nature (see the next example).

As a second step, we calculate bounds $\breve{\mathtt{T}}_{\mathrm{d}}$ and $\hat{\mathtt{T}}_{\mathrm{d}}$ on the sampling period by choosing the Euclidean norm as an error measure and $\varepsilon_{\max} = 1\%$, with the intention to achieve $\eta_{\max} = 1\%$. The calculated sampling bounds are presented in Table III. For the calculation of $\hat{\mathtt{T}}_{\mathrm{d}}$ it has been again assumed that $\mathbb{X} = [-0.4, 0.4]^2$. The results show that the rectangular method needs a fast sampling rate to achieve a stable projection and even a faster sampling to obtain the required performance. The 2^{nd}-order polynomial projection has significantly better bounds due to the 2^{nd}-order accuracy of this method. For the trapezoidal and the Padé cases, the existence of the

[3]*Mean Squared Error*: $\bar{\mathbb{E}}\left\{(y - \hat{y}_{\mathrm{d}})^2\right\} = \lim_{N\to\infty} \frac{1}{N} \sum_{k=0}^{N-1} \mathbb{E}\{(y(k\mathtt{T}_{\mathrm{d}}) - \hat{y}_{\mathrm{d}}(k))^2\}$, i.e. the expected value of the squared estimation error, where $\bar{\mathcal{E}}$ is the generalized expectation operator.

MSE of $\hat{y}_{\mathrm{d}}$

$\mathtt{T}_{\mathrm{d}}$ [s]	Complete	full ZOH	Rectangular	2^{nd}-polynom.	Trapezoidal	Padé $(1,1)$	Adams-Bash.
$2 \cdot 10^{-2}$, (50Hz)	$1.2 \cdot 10^{-8}$	$8.67 \cdot 10^{-2}$	$(*)$	$(*)$	$1.14 \cdot 10^{-1}$	$3.37 \cdot 10^{-1}$	$(*)$
$5 \cdot 10^{-3}$, (0.2kHz)	$6.7 \cdot 10^{-9}$	$1.2 \cdot 10^{-3}$	$(*)$	$2.04 \cdot 10^{-3}$	$9.67 \cdot 10^{-4}$	$3.64 \cdot 10^{-4}$	$1.14 \cdot 10^{-2}$
10^{-4}, (10kHz)	$5.37 \cdot 10^{-8}$	$5.37 \cdot 10^{-8}$	$2.19 \cdot 10^{-7}$	$5.37 \cdot 10^{-8}$	$9.77 \cdot 10^{-8}$	$5.37 \cdot 10^{-8}$	$3.15 \cdot 10^{-7}$

$\hat{\varepsilon}_{\max}$ of $\hat{x}_{\mathrm{d}}$

$\mathtt{T}_{\mathrm{d}}$ [s]	Complete	full ZOH	Rectangular	2^{nd}-polynom.	Trapezoidal	Padé $(1,1)$	Adams-Bash.
$2 \cdot 10^{-2}$, (50Hz)	0.02%	27.43%	$(*)$	$(*)$	4.68%	12.58%	$(*)$
$5 \cdot 10^{-3}$, (0.2kHz)	0.01%	1.71%	$(*)$	1.85%	1.51%	1.25%	12.36%
10^{-4}, (10kHz)	0.06%	0.06%	0.06%	0.07%	0.07%	0.06%	0.16%

$\hat{\eta}_{\max}$ of $\hat{x}_{\mathrm{d}}$

$\mathtt{T}_{\mathrm{d}}$ [s]	Complete	full ZOH	Rectangular	2^{nd}-polynom.	Trapezoidal	Padé $(1,1)$	Adams-Bash.
$2 \cdot 10^{-2}$, (50Hz)	0.02%	78.92%	$(*)$	$(*)$	75.47%	143.37%	$(*)$
$5 \cdot 10^{-3}$, (0.2kHz)	0.01%	5.87%	$(*)$	6.62%	5.47%	2.84%	17.97%
10^{-4}, (10kHz)	0.03%	0.03%	0.06%	0.03%	0.03%	0.03%	0.10%

TABLE II

DISCRETIZATION ERROR OF $\mathcal{S}$, GIVEN IN TERMS OF THE ACHIEVED AVERAGE MSE, $\hat{\varepsilon}_{\max}$ AND $\hat{\eta}_{\max}$ FOR 100 SIMULATIONS. $(*)$ INDICATES UNSTABLE PROJECTION TO THE DISCRETE DOMAIN.

Criteria

	Rectangular	2^{nd}-polynomial	Trapezoidal	Padé $(1,1)$	Adams-Bashforth
$\breve{\mathtt{T}}_{\mathrm{d}}$ [s]	$1.76 \cdot 10^{-3}$, (0.6kHz)	$1.04 \cdot 10^{-2}$, (96.3Hz)	∞	∞	$2.86 \cdot 10^{-3}$, (0.3kHz)
$\hat{\mathtt{T}}_{\mathrm{d}}$ [s]	$1.02 \cdot 10^{-3}$, (1.0kHz)	$2.52 \cdot 10^{-3}$, (0.4kHz)	$3.16 \cdot 10^{-3}$, (0.3kHz)	$> 2.52 \cdot 10^{-3}$, (0.4kHz)	$1.80 \cdot 10^{-3}$, (0.6kHz)

TABLE III

STABILITY ($\breve{\mathtt{T}}_{\mathrm{d}}$) AND PERFORMANCE ($\hat{\mathtt{T}}_{\mathrm{d}}$) BOUNDS USING THE EUCLIDEAN NORM AND $\varepsilon_{\max} = 1\%$.

transformation is always guaranteed because all frozen eigenvalues of $\mathfrak{R}_{\mathrm{LFR}}(\mathcal{S})$ are complex valued and are in the left half-plane.

The derived bounds are used to choose a $\mathtt{T}_{\mathrm{d}}$ for the calculation of the discrete projections. The $\breve{\mathtt{T}}_{\mathrm{d}}$ bounds of Table III represent the stability boundary, therefore $\mathtt{T}_{\mathrm{d}} < \breve{\mathtt{T}}_{\mathrm{d}}$ is used as a new sampling-time in each case. As a next step, discretizations of $\mathfrak{R}_{\mathrm{LFR}}(\mathcal{S})$ with $\mathtt{T}_{\mathrm{d}} = 5 \cdot 10^{-3}$ s, the half of the stability bound $\breve{\mathtt{T}}_{\mathrm{d}}$ for the polynomial method, are calculated. The simulation results

Fig. 4. Prototype of an electronic throttle body for a race bike.

for this case are given in the second row of Table II. The rectangular method again results in an unstable projection, while the Adams-Bashforth method seems to be stable, but its numerical stability is not guaranteed for all trajectories of p_{d}. The trapezoidal and the Padé methods also improve significantly in performance, however the Padé seems to outperform the trapezoidal method due to its faster convergence rate. The achieved $\hat{\varepsilon}_{\max}$ of each approximative method is above the aimed 1% which is in accordance with their $\hat{\mathtt{T}}_{\mathrm{d}}$.

Finally, discretizations of $\mathfrak{R}_{\mathrm{LFR}}(\mathcal{S})$ with $\mathtt{T}_{\mathrm{d}} = 10^{-4}$ s, the $1/10^{\mathrm{th}}$ of the $\breve{\mathtt{T}}_{\mathrm{d}}$ bound for the rectangular method, are calculated and simulated. The results are given in the third row of Table II: the rectangular method converges and also the approximation capabilities of the other methods reach the numerical step-size (10^{-8}) of the continuous-time simulation. By looking at the achieved $\hat{\varepsilon}_{\max}$, all the methods obtain the aimed 1% error performance which is in accordance with their $\hat{\mathtt{T}}_{\mathrm{d}}$ bound. Note that $\hat{\eta}_{\max}$ is also less than 1%, proving the concept that by choosing the sampling period to achieve a small local error, the expected global error will also be small/approximately equal to the aimed bound.

B. Electronic throttle control

In the automotive industry, electronic throttle actuation is regarded as a solution for the air loop control problem for modern combustion engines. A more accurate control of the air inflow to the engine allows better control of the air-fuel mixture with the results of improved combustion and reduced pollution. Motorcycles, especially race bikes, are very sensitive to small changes of the air-fuel mixture which are due to the highly nonlinear behavior of the throttle position. Electronic throttle actuation is an emerging technology in order to optimize the performance of race bikes.

In [22] a recently developed prototype of an *electronic throttle body* (ETB), depicted in Fig. 4, for a race bike has been successfully modeled as an LPV system. With respect to the developed model, a continuous-time gain-scheduled LPV-PID controller was synthesized to regulate the throttle gap based on the demand of the driver. The conceptual diagram of the LPV control loop is illustrated in Fig. 5. Here $r_\theta(t)$ denotes the reference signal for the throttle position, i.e., the demand of the driver, $u_{\rm c}(t)$ is the input of the controller, i.e., the tracking error, $y_{\rm c}$ is the output of the controller, i.e., the PWM signal applied to the DC motor armature, while $\Delta_{\rm v}(t)$ denotes the actual position of the throttle. Analysis of professional drivers' behavior has pointed out that the fastest full-open/full-close maneuver lasts approximately 100 ms, i.e., the reference signal $r_\theta(t)$ is a low frequency signal with a band limit of 20 Hz. By analyzing the dynamical behavior of the throttle body w.r.t. the control synthesis problem, the scheduling signal $p(t)$ of the controller has been selected to be the requested position variation $\Delta r_\theta(t)$. In order to implement a causal filter to estimate this signal, $\Delta r_\theta(t)$ is computed by considering (at the current time instant t_0) the averaged value of the set-point derivative of $r_\theta(t)$ – averaged over a time window $[t_0-\tau, t_0]$ – and propagating it forward over $[t_0, t_0+h]$ by assuming that it remains constant over the latter time interval. The values of h and τ have been experimentally tuned to 7 ms and 100 ms, respectively. The controller has shown good performance both during simulation study and experimental verification. During implementation, a 1 kHz sampling rate has been used, due to physical limitations of the processing unit, and the discrete-time form of the design was obtained via a full ZOH-approach. Here we intend to study how discretization affects the performance of the designed CT controller and how the specific properties of the discretization approaches assist or hamper to obtain an adequate digital implementation of the control design. Furthermore, it is also interesting to check whether the controller can be implemented in DT with a slower sampling rate without sacrificing the performance of the current implementation. The latter would be essential to reduce the cost of the processing unit, providing a cost-effective high-performance solution to the manufacturer.

The gain-scheduled PID controller $\mathcal{K}_{\rm PID}$ was designed based on the interpolation of PID controllers optimized for some fixed throttle positions. Hence for a constant scheduling trajectory $p(t) \equiv \mathtt{p}$, with $\mathtt{p} \in \mathbb{P}$, $\mathcal{K}_{\rm PID}$ is equivalent with an LTI-PID controller having the transfer function

$$G_{\mathtt{p}}(s) = K_{\rm P}\left(1 + \frac{1}{sT_{\rm I}(\mathtt{p})} + \frac{sT_{\rm D}(\mathtt{p})}{1+sT_{\rm D}(\mathtt{p})/N}\right), \tag{48}$$

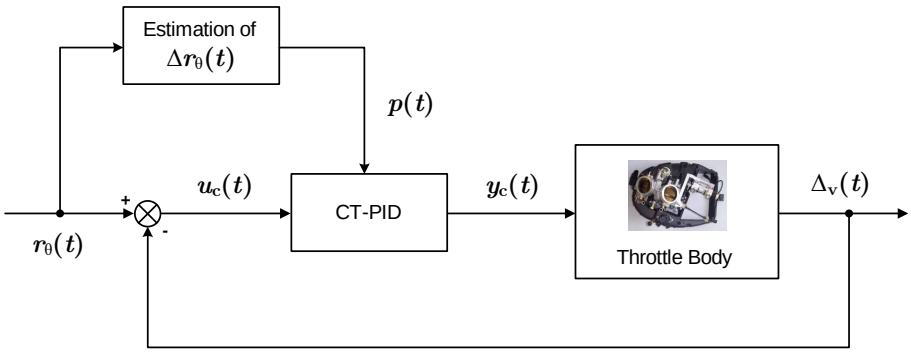

Fig. 5. Conceptual diagram of the LPV-PID based control of the throttle-gap.

where

$$K_{\mathrm{P}} := 3.5 \cdot 10^4,$$

$$T_{\mathrm{D}}(\mathtt{p}) := \underbrace{0.01}_{d_1}\mathtt{p} + \underbrace{0.003}_{d_0}, \quad N := 10,$$

$$T_{\mathrm{I}}(\mathtt{p}) := \underbrace{-0.3074}_{r_3}p^3 + \underbrace{0.6981}_{r_2}p^2 \underbrace{-0.5325}_{r_1}p + \underbrace{0.165}_{r_0}.$$

The interpolated PID controller, with the above given specifications, has a minimal CT-LFR realization in the form of

$$\mathfrak{R}_{\mathrm{LFR}}(\mathcal{K}_{\mathrm{PID}}) = \left[\begin{array}{cc:ccccc:c} 0 & 0 & 0 & 0 & 0 & 0 & 0 & 1 \\ 0 & -\frac{N}{d_0} & 0 & 0 & 0 & -\frac{d_1}{d_0} & \frac{Nd_1}{d_0} & N \\ \hdashline \frac{1}{r_0} & 0 & -\frac{r_1}{r_0} & -\frac{r_2}{r_0} & -\frac{r_3}{r_0} & 0 & 0 & 0 \\ 0 & 0 & 1 & 0 & 0 & 0 & 0 & 0 \\ 0 & 0 & 0 & 1 & 0 & 0 & 0 & 0 \\ 0 & -\frac{N}{d_0} & 0 & 0 & 0 & -\frac{d_1}{d_0} & \frac{Nd_1}{d_0} & N \\ 0 & 0 & 0 & 0 & 0 & 0 & 0 & 1 \\ \hdashline \frac{K_{\mathrm{P}}}{r_0} & -\frac{K_{\mathrm{P}}N}{d_0} & -\frac{K_{\mathrm{P}}r_1}{r_0} & -\frac{K_{\mathrm{P}}r_2}{r_0} & -\frac{K_{\mathrm{P}}r_3}{r_0} & -\frac{K_{\mathrm{P}}d_1}{d_0} & \frac{K_{\mathrm{P}}d_1N}{d_0} & K_{\mathrm{P}}(N+1) \end{array}\right]$$

and with a delta block $\Delta(p)(t) = I_{5\times 5} \cdot p(t)$.

First, we investigate the approximation of the behavior of $\mathfrak{R}_{\mathrm{LFR}}(\mathcal{K}_{\mathrm{PID}})$ w.r.t. the proposed discretization approaches using the physically possible 1 kHz maximum of the sampling frequency. According to this, consider $\mathfrak{R}_{\mathrm{LFR}}(\mathcal{K}_{\mathrm{PID}})$ in the exact ZOH setting of Fig. 3b with sampling period $\mathtt{T}_{\mathrm{d}} = 10^{-3}$ s. Based on the discretization approaches of Sec. IV, DT approximations of $\mathfrak{R}_{\mathrm{LFR}}(\mathcal{K}_{\mathrm{PID}})$ have been calculated similarly as in the previous example. Note that in the considered discretization setting we only aim at the stand-alone discretization of the given LFR,

which refers to an open-loop setting. Therefore, in order to demonstrate the performance of the resulting DT controllers, we first focus on their open-loop simulation error and only later we will test their closed-loop behavior. In order to facilitate an open-loop comparison of the CT and DT-PIDs, the continuous-time closed loop system, depicted on Fig. 5, has been simulated on the time interval $[0, 1]$ with zero initial conditions in MATLAB. During the simulation a sinusoidal reference signal $r_\theta(t) = \frac{1}{2} + \frac{1}{2}\sin(2.5t)$ has been applied and the ODE45 numerical solver has been used with a variable step size having a maximum of 10^{-6}. The results of this simulation are depicted in Fig. 6, where in the bottom figure it can be seen that the red throttle demand has been well tracked by the actual throttle position given in blue. All signals of the closed loop have been recorded with a sampling period of 10^{-6} s. These signals were down sampled to $\mathtt{T}_\mathrm{d} = 10^{-3}$ s and the resulting DT signals $u_\mathrm{cd}(k) = u_\mathrm{c}(k\mathtt{T}_\mathrm{d})$ and $p_\mathrm{d}(k) = p(k\mathtt{T}_\mathrm{d})$ have been used to simulate the response of the obtained discrete-time controller by each proposed methods. The resulting DT output signals $\hat{y}_\mathrm{c}$ are depicted in Fig. 7a. The achieved MSE of $\hat{y}_\mathrm{cd}$ has been calculated w.r.t. the sampled output $y_\mathrm{c}(k\mathtt{T}_\mathrm{d})$ of $\mathfrak{R}_\mathrm{LFR}(\mathcal{K}_\mathrm{PID})$ and is presented in Table IV. The relative worst-case maximum local error $\hat{\varepsilon}_\mathrm{max}$ and global error $\hat{\eta}_\mathrm{max}$ of the DT state-signals $\hat{x}_\mathrm{d}$ associated with the DT controllers have been also computed w.r.t. to the state-signals of $\mathfrak{R}_\mathrm{LFR}(\mathcal{K}_\mathrm{PID})$ and are presented in Table IV. During the calculation of $M_\mathbf{x}^\mathrm{max}$, $\mathbb{X} = [-5 \cdot 10^{-3}, 5 \cdot 10^{-3}]^2$ was used in accordance with the amplitudes of the state-signals of $\mathfrak{R}_\mathrm{LFR}(\mathcal{K}_\mathrm{PID})$ during the CT simulation.

From Table IV it is apparent that the rectangular, the 2^nd-order polynomial and the 3-step Adams-Bashforth approaches do not provide numerically convergent approximations while the complete approach has a negligible approximation error as expected. The Padé $(1, 1)$ approach provides the best result among the approximative methods while the trapezoidal one gives somewhat moderate results. The large MSE values of the output approximation are due to the extremely large value of y_c around $t = 0.01$, see the upper part of Fig. 6. As the trapezoidal approach averages the state-evolution over the sample interval, it inherently has a relatively large error ($\hat{\varepsilon}_\mathrm{max} = 36\%$) for such huge variations. This is why the Padé $(1, 1)$ approach achieves a better performance ($\hat{\varepsilon}_\mathrm{max} = 2.36\%$) as it approximates the complete approach rather than the state-evolution itself. In line with the previous observations in [22], the full ZOH approach also provides a convergent approximation, however with the worst MSE. This immediately shows that by applying the Padé $(1, 1)$ or the trapezoidal approach in the implementation of the throttle

controller, the performance loss of the CT design can be decreased.

To analyze the approximation capabilities of the methods, we next can calculate the bounds $\breve{\mathtt{T}}_{\mathrm{d}}$ and $\hat{\mathtt{T}}_{\mathrm{d}}$ on the sampling period by choosing the Euclidean norm as an error measure and $\varepsilon_{\max} = 10\%$, with the intention to achieve $\eta_{\max} = 10\%$. Note that $\breve{\mathtt{T}}_{\mathrm{d}}$ is infinite as the PID controller contains an integrator part, which is not asymptotically stable. The calculated $\hat{\mathtt{T}}_{\mathrm{d}}$ bounds are presented in Table V. During the calculation of $\hat{\mathtt{T}}_{\mathrm{d}}$, the regions $\mathbb{P} = [0, 1]$ and $\mathbb{U} = [-1, 1]$ have been used which were obtained from the simulation results of the CT-PID controller (see Fig. 6).

As a next step, discretization of $\mathfrak{R}_{\mathrm{LFR}}(\mathcal{K}_{\mathrm{PID}})$ has been computed via all approaches using $\mathtt{T}_{\mathrm{d}} = 2.5 \cdot 10^{-4}$, the sampling period where the 2^{nd}-order polynomial approach achieves the aimed worst-case numerical error. As we can see from Table IV, all approaches improve in performance, the rectangular method becomes convergent, while the 3-step Adams-Bashforth approach still diverges. Comparing the maximum of the LUT error, we can see that, as expected, the 2^{nd}-order polynomial approach achieves the aimed $\varepsilon_{\max} = 10\%$. Due to its faster convergence rate, the Padé $(1, 1)$ method has even better performance in all measures than the 2^{nd}-order polynomial. However, the Trapezoidal approach still has a large error, even larger than the rectangular approach in almost all measures, which is due to its erratic behavior around $t = 0.01$. On the other hand, respecting the bounds, its maximum LUT error is below 10%. An also interesting observation is that contrary to the previous example, the full ZOH approach has a poor performance, especially in terms of the MSE of the output, compared to the other methods. This clearly shows the unpredictable behavior of this discretization scheme.

Next, we investigate discretization with all methods using $\mathtt{T}_{\mathrm{d}} = 10^{-4}$. From Table IV, it follows that all methods with this sampling period achieve the aimed $\eta_{\max} = 10\%$ bound and in case of the Padé $(1, 1)$ and the 2^{nd}-order polynomial approaches the MSE of $\hat{y}_{\mathrm{cd}}$ becomes negligible compared to the amplitude of y_{c}. However, the Trapezoidal and the Adams-Bashforth approaches perform poorly, especially in terms of $\hat{\varepsilon}_{\max}$ and $\hat{\eta}_{\max}$. Even the full ZOH approach seems to perform better in terms of these error measures. From the preformed open-loop simulation it seems that the Padé $(1, 1)$ approach provides the best discretization of the LPV-PID controller for all practically interesting values of $\mathtt{T}_{\mathrm{d}}$ and it can be shown that it remains to perform better than the Trapezoidal approach even for $\mathtt{T}_{\mathrm{d}} > 10^{-3}$. This seems to give the conclusion that the

Padé $(1,1)$ approach provided DT LPV controller will perform better than the one based on the trapezoidal approach. To investigate this, the closed-loop behavior of the DT LPV controllers obtained by all approaches has been analyzed w.r.t a realistic gas profile, see Fig. 8. This gas profile in terms of demanded throttle position has been recorded during a test track lap performed by a professional driver. Using this gas profile the CT LPV-PID controller has been simulated together with its DT projection via all approaches under various values of $\mathtt{T}_\mathrm{d}$. The results are visualized in Fig. 10 in terms of the MSE of $\hat{y}_\mathrm{cd}(k)$ w.r.t. the gas profile $r_\theta(k\mathtt{T}_\mathrm{d})$. In this figure, the performance of the CT controller is given by a black solid line, while the achieved performance of the DT controllers, produced by each discretization method, is given for equidistant values of $\mathtt{T}_\mathrm{d}$ on the range $[10^{-4}, 2\cdot 10^{-3}]$. The response of the simulated closed-loop system is given on Fig. 9 w.r.t. to the CT-PID and the controllers provided by the convergent approaches for $\mathtt{T}_\mathrm{d} = 10^{-3}$. From these figures it becomes evident that the Trapezoidal method provides an excellent steady performance in terms of tracking for all values of $\mathtt{T}_\mathrm{d}$ in the considered region. The Padé $(1,1)$ method in closed-loop performs significantly worse than during the open-loop simulations as between $4\cdot 10^{-4}$ and 10^{-3} even the full ZOH approach performs better. At $\mathtt{T}_\mathrm{d} = 1.5\cdot 10^{-3}$ the full ZOH approach based controller is not able to stabilize the loop any more which is quickly followed by the divergence of the Padé $(1,1)$ method based controller at $\mathtt{T}_\mathrm{d} = 1.6\cdot 10^{-3}$. As expected from the open-loop simulations, the Adams-Bashforth approach based design only provides a stable, but well-performing controller at $\mathtt{T}_\mathrm{d} = 10^{-4}$ and the 2^{nd}-order polynomial approach starts to diverge above $\mathtt{T}_\mathrm{d} = 5\cdot 10^{-4}$. What is interesting is that the rectangular method performs well till $\mathtt{T}_\mathrm{d} = 7\cdot 10^{-4}$ and then it quickly becomes unstable. As an overall conclusion it follows that contrary to the open-loop simulation study it turns out that the Trapezoidal approach provides the best DT controller in terms of tracking, which is followed by the full ZOH approach, while the Padé $(1,1)$ does not seem to be an attractive choice at all. Explanation of this result lies in the fact that the considered discretization setting and the provided analysis in this paper have focused on the stand alone discretization of an open-loop LPV system. In that case, we could see that the developed methods in this example achieved the performance suggested by the theory. However, as is well-known in the LTI case, discretization w.r.t. a system in a closed-loop considering a closed-loop performance measure is a different problem setting. This underlines that the results reported in this paper are the first steps

MSE of $\hat{y}_{\mathrm{cd}}$

$\mathtt{T}_{\mathrm{d}}$ [s]	Complete	full ZOH	Rectangular	2^{nd}-polynom.	Trapezoidal	Padé $(1,1)$	Adams-Bash.
10^{-3}, (1kHz)	$6.20 \cdot 10^{-19}$	$1.08 \cdot 10^{7}$	$(*)$	$(*)$	$7.46 \cdot 10^{6}$	$6.62 \cdot 10^{4}$	$(*)$
$2.5 \cdot 10^{-4}$, (4kHz)	$6.23 \cdot 10^{-19}$	$1.03 \cdot 10^{6}$	$1.83 \cdot 10^{5}$	$1.23 \cdot 10^{3}$	$4.60 \cdot 10^{5}$	$2.15 \cdot 10^{2}$	$(*)$
10^{-4}, (10kHz)	$6.19 \cdot 10^{-19}$	$1.70 \cdot 10^{5}$	$2.57 \cdot 10^{4}$	$2.52 \cdot 10^{1}$	$7.28 \cdot 10^{4}$	$5.47 \cdot 10^{0}$	$1.00 \cdot 10^{5}$

$\hat{\varepsilon}_{\max}$ of $\hat{x}_{\mathrm{d}}$

$\mathtt{T}_{\mathrm{d}}$ [s]	Complete	full ZOH	Rectangular	2^{nd}-polynom.	Trapezoidal	Padé $(1,1)$	Adams-Bash.
10^{-3}, (1kHz)	0.00%	25.35%	$(*)$	$(*)$	36.00%	2.36%	$(*)$
$2.5 \cdot 10^{-3}$, (4kHz)	0.00%	3.78%	1.99%	0.16%	9.02%	0.06%	$(*)$
10^{-4}, (10kHz)	0.00%	0.74%	0.33%	0.01%	3.61%	0.01%	6.95%

$\hat{\eta}_{\max}$ of $\hat{x}_{\mathrm{d}}$

$\mathtt{T}_{\mathrm{d}}$ [s]	Complete	full ZOH	Rectangular	2^{nd}-polynom.	Trapezoidal	Padé $(1,1)$	Adams-Bash.
10^{-3}, (1kHz)	0.00%	31.72%	$(*)$	$(*)$	24.51%	2.36%	$(*)$
$2.5 \cdot 10^{-3}$, (4kHz)	0.00%	8.95%	3.73%	0.31%	8.06%	0.13%	$(*)$
10^{-4}, (10kHz)	0.00%	3.54%	1.40%	0.05%	3.45%	0.02%	6.95%

TABLE IV

DISCRETIZATION ERROR OF $\mathcal{S}$, GIVEN IN TERMS OF THE ACHIEVED MSE, $\hat{\varepsilon}_{\max}$ AND $\hat{\eta}_{\max}$ FOR THE INVESTIGATED STATE TRAJECTORY. $(*)$ INDICATES UNSTABLE PROJECTION TO THE DISCRETE DOMAIN.

Criteria

	Rectangular	2^{nd}-polynomial	Trapezoidal	Padé $(1,1)$	Adams-Bashforth
$\hat{\mathtt{T}}_{\mathrm{d}}$ [s]	$1.26 \cdot 10^{-4}$, (7.93kHz)	$2.42 \cdot 10^{-4}$, (4.12kHz)	$3.06 \cdot 10^{-4}$, (3.27kHz)	$> 2.42 \cdot 10^{-4}$, (4.12kHz)	$2.09 \cdot 10^{-4}$, (4.78kHz)

TABLE V

PERFORMANCE ($\hat{\mathtt{T}}_{\mathrm{d}}$) BOUNDS USING THE EUCLIDEAN NORM AND $\varepsilon_{\max} = 10\%$.

towards providing theoretically well-understood solutions for the DT implementation of CT-LPV controllers preserving their closed-loop performance, which is the aim of future research.

VII. CONCLUSIONS

In this paper, discretization approaches of *linear fractional representations* (LFR's) of LPV systems were introduced using an exact ZOH setting where the variation of the state coupled by the scheduling dependent Δ-block is not restricted inside the sampling interval. This provides an advantage over existing methods to reduce the introduced discretization error. The developed

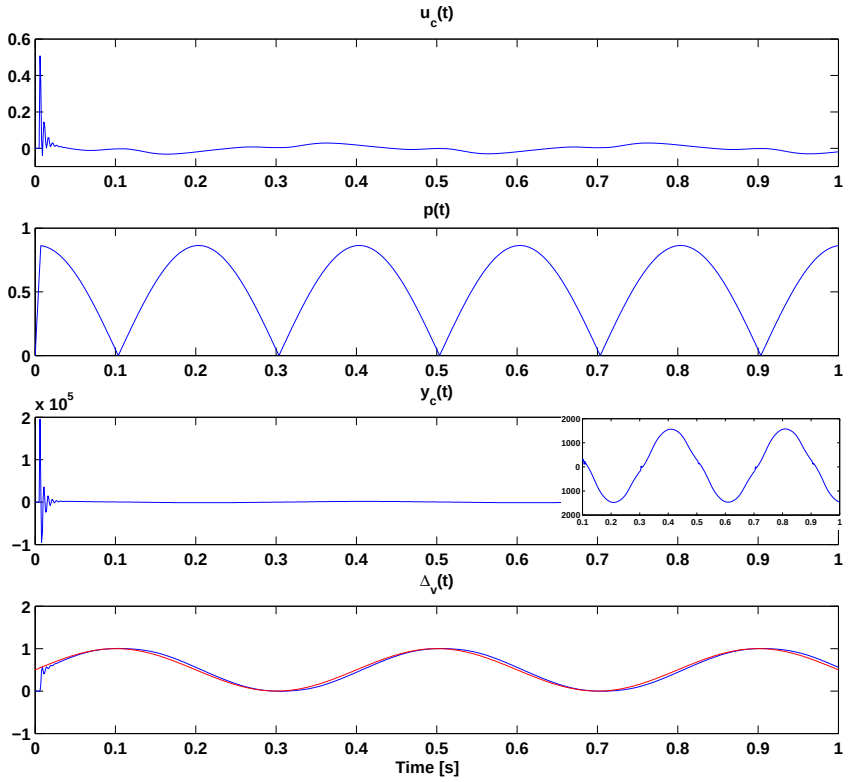

Fig. 6. Closed-loop response of the system with the CT-PID controller for a sinusoidal gas profile: controller input (tracking error) $u_{\mathrm{c}}(t)$, scheduling signal $p(t)$, controller output (actuation) $y_{\mathrm{c}}(t)$, system output $\Delta_{\mathrm{v}}(t)$ (blue, bottom subfigure) and the tracked gas profile (red, bottom subfigure).

approaches were analyzed in terms of applicability and numerical properties, giving an overview of which methods are attractive depending on the aim and achievable sampling period of the discretization. Illustrative examples were provided to give insight into the derived methods and their properties.

REFERENCES

[1] A. Packard, "Gain scheduling via linear fractional transformations," *Systems & Control Letters*, vol. 22, no. 2, pp. 79–92, 1994.

[2] C. W. Scherer, "Mixed $\mathcal{H}_2/\mathcal{H}_\infty$ control for time-varying and linear parametrically-varying systems," *Int. Journal of Robust and Nonlinear Control*, vol. 6, no. 9-10, pp. 929–952, 1996.

[3] K. Zhou, J. C. Doyle, and K. Glover, *Robust and Optimal Control*. Prentice-Hall, 1995.

[4] H. Hanselmann, "Implementation of digital controllers - A survey," *Automatica*, vol. 23, no. 1, pp. 7–32, 1987.

[5] J. Kim, D. G. Bates, and I. Postletwaite, "Robustness analysis of linear periodic time-varying systems subject to structured uncertainty," *Systems & Control Letters*, vol. 55, pp. 719–725, 2006.

[6] L. Ma and P. Iglesias, "Robustness analysis of a self-oscillating molecular network in a dictyostelium discoideum," in *Proc. of the 41th IEEE Conf. on Decision and Control*, Las Vegas, Nevada, USA, Dec. 2002, pp. 2538–2543.

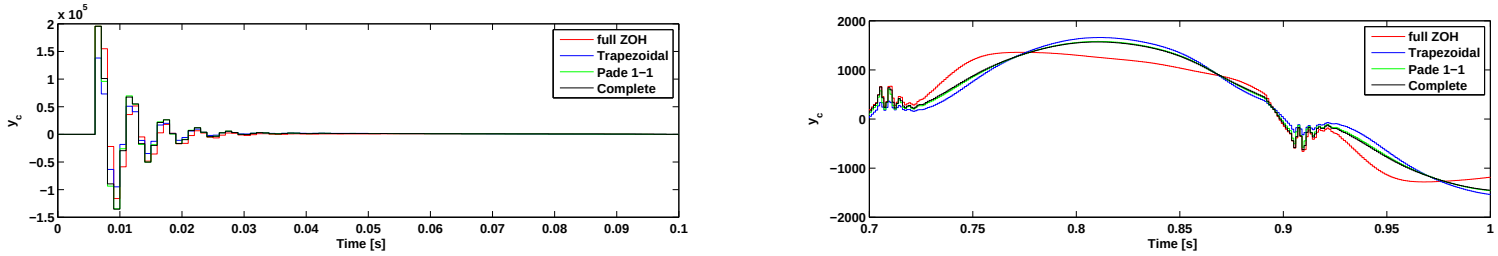

(a) $\mathrm{T_d} = 10^{-3}$

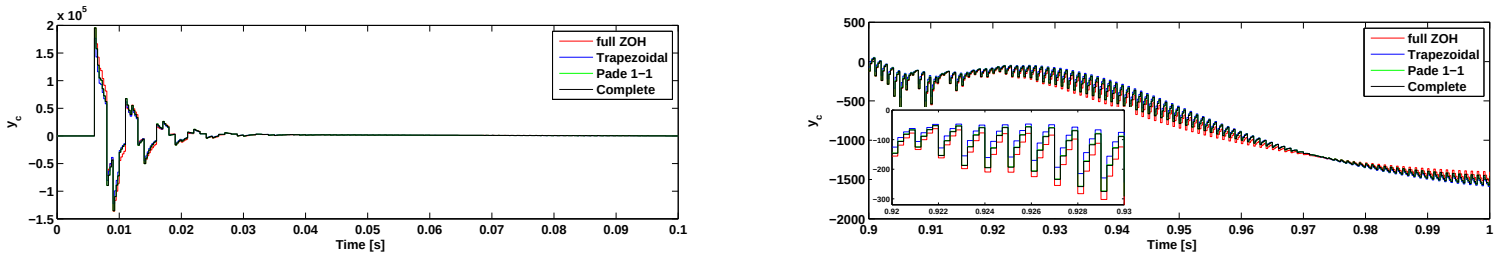

(b) $\mathrm{T_d} = 2.5 \cdot 10^{-4}$

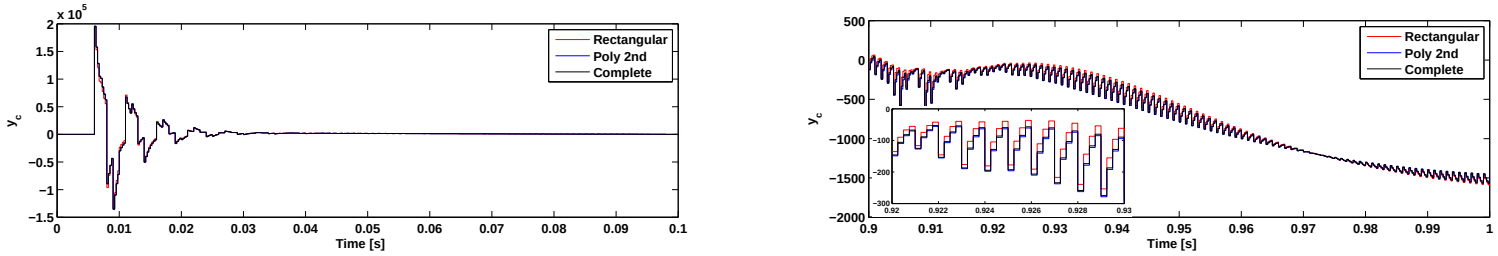

(c) $\mathrm{T_d} = 2.5 \cdot 10^{-4}$

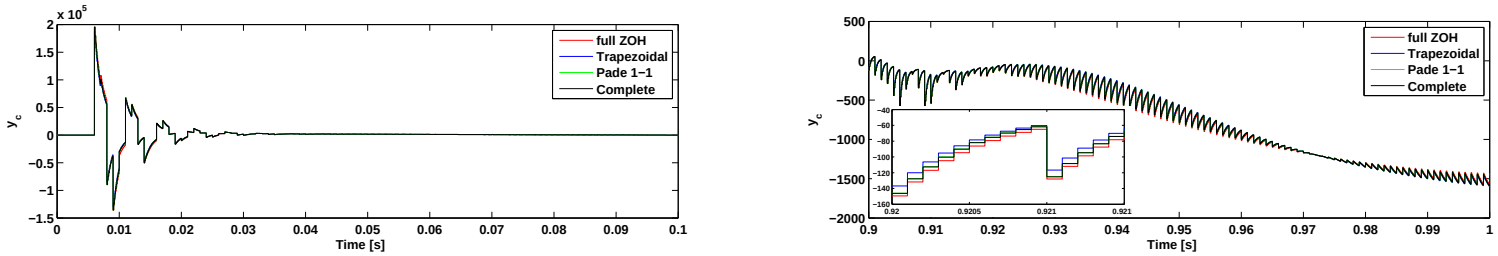

(d) $\mathrm{T_d} = 10^{-4}$

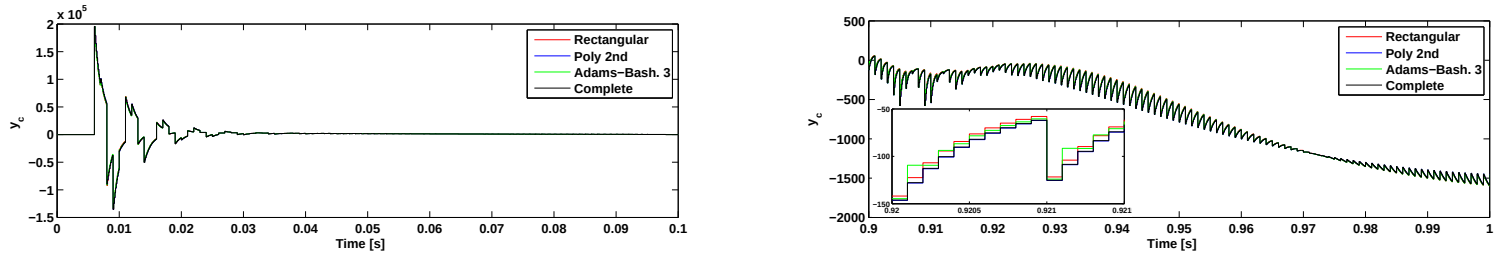

(e) $\mathrm{T_d} = 2.5 \cdot 10^{-4}$

Fig. 7. Open loop simulation results of the discretized PID controller using the proposed approaches and different sampling periods $\mathrm{T_d}$.

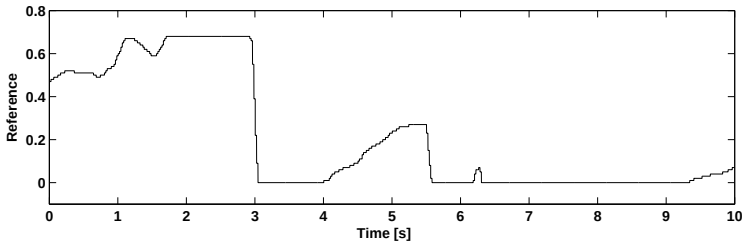

Fig. 8. Driver gas request (demanded throttle position) measured in a test track lap.

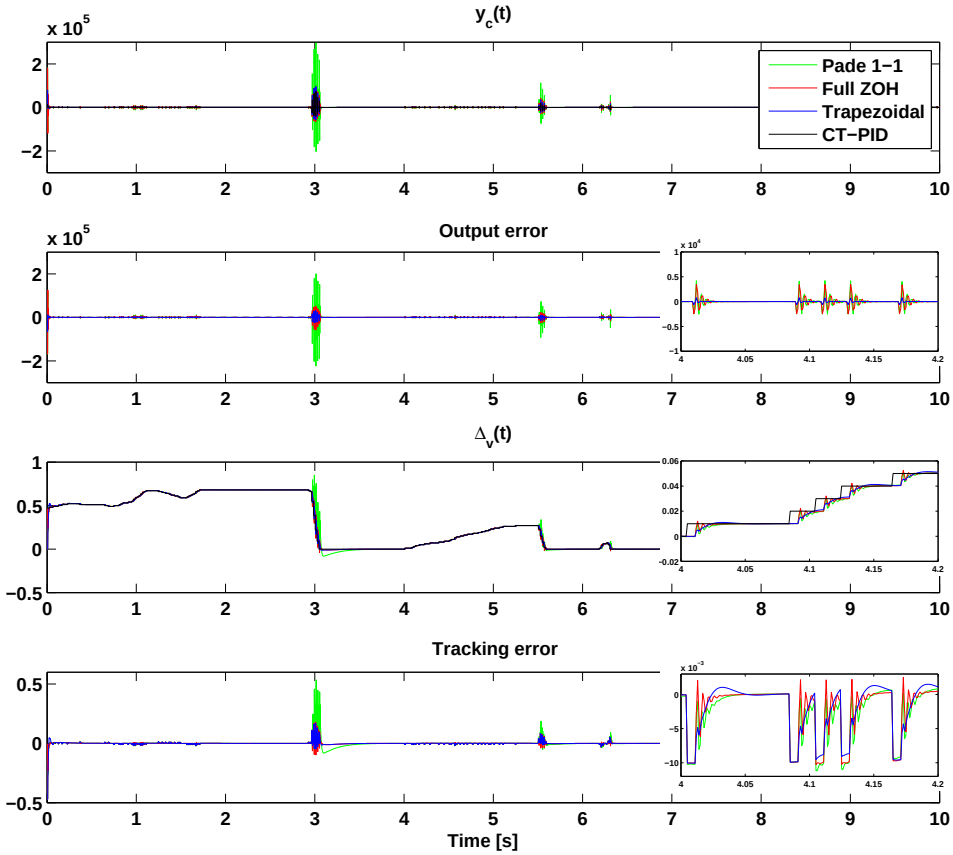

Fig. 9. Closed-loop response of the system with the CT-PID controller (black) and with its discrete-time projections for a real gas profile. The results are plotted in terms of the controller output signal (actuation) $y_{\rm c}$, the difference of the output of the DT controller w.r.t. the CT output, the $\Delta_{\rm v}(t)$ throttle position (system output) and the tracking error of the throttle position.

[7] D. Peaucelle, C. Farges, and D. Arzelier, "Robust LFR-based technique for stability analysis of limit cycles," in *Proc. of the IFAC Symposium ALCOSP'07/PSYCO'07*, St. Petersburg, Russia, Aug. 2007.

[8] N. Imbert, "Robustness analysis of a launcher attitude controller via μ-analysis," in *Proc. of the 15th IFAC Symposium on Automatic Control in Aerospace*, Bologna, Italy, Sept. 2001, pp. 429–434.

[9] P. C. Pellanda, P. Apkarian, and H. D. Tuan, "Missile autopilot design via a multi-channel LFT/LPV control method," *Int. Journal of Robust and Nonlinear Control*, vol. 12, no. 1, pp. 1–20, 2002.

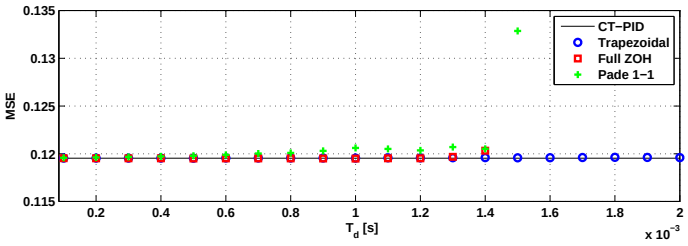

(a)

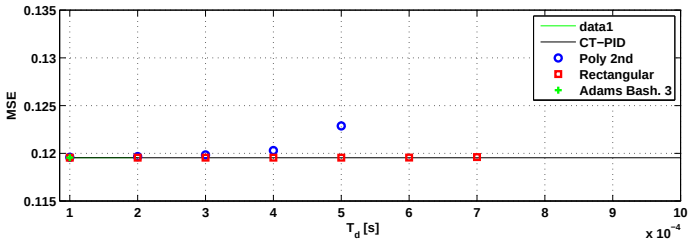

(b)

Fig. 10. Closed-loop mean-squared tracking error with the controllers provided by the discretization methods under different sampling periods $\mathtt{T_d}$.

[10] G. Ferreres, "Reduction of dynamic LFT systems with LTI model uncertainties," *Int. Journal of Robust and Nonlinear Control*, vol. 14, no. 3, pp. 307–323, 2004.

[11] R. Tóth, F. Felici, P. S. C. Heuberger, and P. M. J. Van den Hof, "Crucial aspects of zero-order-hold LPV state-space system discretization," in *Proc. of the 17th IFAC World Congress*, Seoul, Korea, July 2008, pp. 3246–3251.

[12] R. Tóth, *Modeling and Identification of Linear Parameter-Varying Systems*, ser. Lecture Notes in Control and Information Sciences, Vol. 403. Springer-Germany, 2010.

[13] K. E. Atkinson, *An Introduction to Numerical Analysis*. John Wiley and Sons, 1989.

[14] C. Arévalo and G. Söderlind, "Convergence of multistep discretizations of DAEs," *BIT Numerical Mathematics*, vol. 35, no. 2, pp. 143–168, 1995.

[15] E. Hairer and G. Wanner, *Solving ordinary differential equations II: Stiff and differential-algebraic problems*. Springer Verlag, 2010, vol. 14.

[16] R. Tóth, M. Lovera, P. S. C. Heuberger, and P. M. J. Van den Hof, "Discretization of linear fractional representations of LPV systems," in *Proc. of the 48th IEEE Conf. on Decision and Control*, Shanghai, China, Dec. 2009, pp. 7424–7429.

[17] K. J. Åström and B. Wittenmark, *Computer controlled systems*. Prentice-Hall, 1990.

[18] R. Tóth, M. Lovera, M. Corno, P. S. C. Heuberger, and P. M. J. Van den Hof, "On the discretization of linear fractional representations of LPV systems: Detailed derivation of the formulas," Delft University of Tech., Tech. Rep. 11-037, 2011.

[19] A. L. Tits and M. K. H. Fan, "On the small-μ theorem," *Automatica*, vol. 31, pp. 1199–1201, 1995.

[20] C. B. Moler and C. F. Van Loan, "Nineteen dubious ways to compute the exponential of a matrix, twenty-five years later," *SIAM Review*, vol. 45, no. 1, pp. 3–49, 2003.

[21] B. N. Datta, *Numerical methods for linear control systems*. Elsevier, 2004.

[22] M. Corno, M. Tanelli, S. M. Savaresi, L. Fabbri, and L. Nardo, "Electronic throttle control for ride-by-wire in sport motorcycles," in *Proc. of the 17th IEEE Int. Conf. on Control Applications*, San Antonio, Texas, USA, 2008, pp. 233–238.